Screening of TRPC Channel Activators Identifies

Novel Neurotrophic Piperazine Compounds

Seishiro Sawamura, Masahiko Hatano, Yoshinori Takada, Kyosuke Hino,

Tetsuya Kawamura, Jun Tanikawa, Hiroshi Nakagawa, Hideharu Hase, Akito Nakao,

Mitsuru Hirano, Rachapun Rotrattanadumrong, Shigeki Kiyonaka, Masayuki X. Mori,

Motohiro Nishida, Yaopeng Hu, Ryuji Inoue, Ryu Nagata and Yasuo Mori

Department of Synthetic Chemistry and Biological Chemistry, Graduate School of
Engineering, Kyoto University, Kyoto, Japan (S.S., M.H., Y.T., H.H., M.H., R.R., S.K.,
M.M., Y.M.); Department of Technology and Ecology, Hall of Global Environmental
Studies, Kyoto University, Kyoto, Japan (S.K., Y.M.); Sumitomo Dainippon Pharma Co.,
Ltd. (Y.T., K.H., T.K., J.T., H.N., R.N.); Division of Systems Medical Science, Institute
for Comprehensive Medical Science, Fujita Health University, Toyoake, Japan (A.N.);
Division of Cardiocirculatory Signaling, Okazaki Institute for Integrative Bioscience
(National Institute for Physiological Sciences), National Institutes of Natural Sciences,
Japan (M.N.); Department of Physiology, School of Medicine, Fukuoka University
Fukuoka, Japan (Y.H., R.I.)

Running title:

Neurotrophic Action of Novel TRPC Channel Activators

Address for correspondence:

Yasuo Mori, Ph.D.

Laboratory of Molecular Biology, Department of Synthetic Chemistry and Biological Chemistry, Graduate School of Engineering, Kyoto University, Katsura Campus, Nishikyo-ku, Kyoto 615-8510, Japan.

Tel: 81-75-383-2761, Fax: 81-75-383-2765

E-mail: mori@sbchem.kyoto-u.ac.jp

Number of text pages: 56

Tables: 0

Figures: 9

References: 69

Number of words in the Abstract: 247

Number of words in the Introduction: 750

Number of words in the Discussion: 1708

Abbreviations: BDNF, brain-derived neurotrophic factor; BAPTA, 1,2-bis(2-aminophenoxy)ethane-N,N,N',N'-tetraacetic acid; $[Ca^{2+}]_i$, intracellular Ca^{2+} concentration; CaMK, Ca^{2+}/calmodulin-dependent protein kinase; capsazepine, N-[2-(4-chlorophenyl)ethyl]-1,3,4,5-tetrahydro-7,8-dihydroxy-2H-2-benzazepine-2-carbothioamide; CGNs, cerebellar granule neurons; CNS, central nervous system;

2

CREB, cAMP response element-binding protein; DAG, diacylglycerol; DIV, days *in vitro*; DMEM, Dulbecco's modified Eagle's medium; EGFP, enhanced green fluorescent protein; FMP, FLIPR® membrane potential; HEK, human embryonic kidney; KN-93, *N*-[2-[[[3-(4-chlorophenyl)-2-propenyl]methylamino]methyl]phenyl]-*N*-(2-hydroxyethyl)-4-methoxybenzenesulphonamide; MAPK, mitogen-activated protein kinase; MEK, MAPK/ERK kinase; ML-7, hexahydro-1-[(5-iodo-1-naphthalenyl)sulfonyl]-1*H*-1,4-diazepine hydrochloride; MLCK, myosin light chain kinase; NFAT, nuclear factor of activated T-cells; Norad, noradrenaline; OAG, 1-oleoyl-2-acetyl-*sn*-glycerol; PKC, protein kinase C; PLC, phospholipase C; RT-PCR, reverse transcriptase-polymerase chain reaction; Trk, tropomyosin-related kinase; PD98059, 2-(2-amino-3-methoxyphenyl)-4*H*-1-benzopyran-4-one; PI, propidium iodide; PPZ1, [4-(5-chloro-2-methylphenyl)piperazin-1-yl](3-fluorophenyl)methanone; PPZ2, 2-[4-(2,3-dimethylphenyl)piperazin-1-yl]-*N*-(2-ethoxyphenyl)acetamide; SK&F 96365, 1-[2-(4-methoxyphenyl)-2-[3-(4-methoxyphenyl)propoxy]ethyl-1*H*-imidazole hydrochloride; STO-609, 7-oxo-7*H*-benzimidazo[2,1-a]benz[de]isoquinoline-3-carboxylic acid; TRP, transient receptor potential; U73122, 1-[6-[[(17β)-3-methoxyestra-1,3,5(10)-trien-17-yl]amino]hexyl]-1*H*-pyrrole-2,5-dione; U73343, 1-[6-[[(17β)-3-methoxyestra-1,3,5(10)-trien-17-yl]amino]hexyl]-2,5-pyrrolidinedione

3

Abstract

Transient receptor potential canonical (TRPC) proteins form Ca^{2+}-permeable cation channels activated upon stimulation of metabotropic receptors coupled to phospholipase C. Among the TRPC subfamily, TRPC3 and TRPC6 channels activated directly by diacylglycerol (DAG) play important roles in brain-derived neurotrophic factor (BDNF) signaling, promoting neuronal development and survival. In various disease models, BDNF restores neurological deficits, but its therapeutic potential is limited by its poor pharmacokinetic profile. Elucidation of a framework for designing small molecules, that elicit BDNF-like activity via TRPC3 and TRPC6, establishes a solid basis to overcome this limitation. We discovered, through library screening, a group of piperazine-derived compounds that activate DAG-activated TRPC3/TRPC6/TRPC7 channels. The compounds [4-(5-chloro-2-methylphenyl)piperazin-1-yl](3-fluorophenyl)methanone (PPZ1) and 2-[4-(2,3-dimethylphenyl)piperazin-1-yl]-*N*-(2-ethoxyphenyl)acetamide (PPZ2) activated, in a dose-dependent manner, recombinant TRPC3/TRPC6/TRPC7 channels but not other TRPCs in human embryonic kidney cells. PPZ2 activated native TRPC6-like channels in smooth muscle cells isolated from the rabbit portal vein. Also, PPZ2 evoked cation currents and Ca^{2+} influx in rat cultured central neurons. Strikingly, both compounds induced BDNF-like neurite growth and neuroprotection, which were abolished by a knockdown or inhibition of TRPC3/TRPC6/TRPC7 in cultured neurons. Inhibitors of Ca^{2+} signaling pathways except calcineurin impaired neurite outgrowth promotion induced by PPZ compounds. PPZ2 increased activation of the Ca^{2+}-dependent transcription factor, cAMP response element-binding protein (CREB). These findings suggest that Ca^{2+} signaling mediated by activation of DAG-activated

TRPC channels underlies neurotrophic effects of PPZ compounds. Thus, piperazine-derived activators of DAG-activated TRPC channels provide important insights for future development of a new class of synthetic neurotrophic drugs.

5

Introduction

Brain-derived neurotrophic factor (BDNF) is the most abundant and widely distributed neurotrophin in the mammalian central nervous system (CNS). BDNF binds to tropomyosin-related kinase B (TrkB), a receptor tyrosine kinase, to stimulate various intracellular signaling pathways mediated by mitogen-activated protein kinase (MAPK), phosphatidylinositol 3-kinase, or phospholipase C (PLC) γ (Huang and Reichardt, 2003; Reichardt, 2006; Zhang et al., 2012). Through these intracellular signaling pathways, BDNF exerts neurotrophic functions such as promoting neuronal growth and survival or modulating synaptic transmission and plasticity (Huang and Reichardt, 2001; Park and Poo, 2013). BDNF administration showed beneficial effects in models for various diseases such as Alzheimer's disease, Parkinson's disease, depression, and schizophrenia (Nagahara and Tuszynski, 2011; Autry and Monteggia, 2012). However, its pharmacokinetic properties including short plasma half-life and poor blood brain barrier penetration limit its therapeutic applications (Poduslo and Curran, 1996). Therefore, discovery of small molecules that mimic the neurotrophic actions of BDNF would be a promising therapeutic strategy for neurological and psychiatric disorders.

Drosophila melanogaster transient receptor potential (TRP) protein and its homologs are putative six-transmembrane polypeptide subunits that form tetrameric Ca^{2+}-permeable non-selective cation channels (Clapham, 2003; Clapham et al., 2005; Nilius and Szallasi, 2014). Mammalian TRP channels are grouped into six related subfamilies, TRPC, TRPV, TRPM, TRPA, TRPP, and TRPML. TRP channels are activated by diverse stimuli including receptor stimulation, heat, osmotic pressure, mechanical stress and environmental irritants from the extracellular and intracellular

milieu. "Canonical" TRPC subfamily comprises seven members (TRPC1–C7), highly expressed in the mammalian CNS and mediating cation influx induced by activation of PLC-coupled metabotropic receptors such as G protein-coupled receptors and receptor tyrosine kinases (Vazquez et al., 2004; Abramowitz and Birnbaumer, 2009). PLC hydrolyzes phosphatidylinositol 4,5-bisphosphate to form diacylglycerol (DAG) (Fig. 1A) and inositol 1,4,5-trisphosphate. In addition to their well-known activation of protein kinase C (PKC), a kinase regulating a plethora of biological functions (Nishizuka, 1995), DAG and its analogues also activate the closely related TRPC subtypes, TRPC3, TRPC6, and TRPC7 (Hofmann et al., 1999).

In the CNS, TRPC3 and TRPC6 modulate neurotransmission, synaptic plasticity, neuronal development, and neuronal survival (Abramowitz and Birnbaumer, 2009; Nilius and Szallasi, 2014). Previous studies further showed that TRPC3 and TRPC6 are important for growth cone turning, spine formation and neuronal survival induced by BDNF stimulation in neurons (Li et al., 2005; Amaral and Pozzo-Miller, 2007; Jia et al., 2007). It has been suggested that, with BDNF stimulation, TRPC3 and TRPC6 are activated by the PLC pathway via TrkB (Li et al., 1999, Amaral and Pozzo-Miller, 2007; Jia et al., 2007). This cascade contributes to increased intracellular Ca^{2+} concentration ($[Ca^{2+}]_i$) and subsequent Ca^{2+}-dependent activation of such intracellular signaling molecules as MAPKs, Ca^{2+}/calmodulin-dependent protein kinases (CaMKs) and Ca^{2+}-dependent transcription factor cAMP response element-binding protein (CREB), all of which play beneficial roles on neuronal functions (Shaywitz and Greenberg, 1999; Agell et al., 2002; Jia et al., 2007; Wayman et al., 2008). The importance of TRPC6 has been also recognized through investigation of hyperforin (Fig. 1A), an active ingredient of St. John's wort, which is a widely used and well-investigated medicinal

plant (Wolfle et al., 2014). Hyperforin is a multi-target compound that modulates various molecular functions and exerts various beneficial effects, showing anti-microbial, anti-inflammatory, anti-cancer and antidepressant activity (Russo et al., 2014). It has been previously reported that hyperforin exerts antidepressant and neurotrophic effects via activation of TRPC6 in neurons (Leuner et al., 2007; Leuner et al., 2013; Griesi-Oliveira et al., 2014). However, the activity of hyperforin remains controversial: recent publication implicates that the protonophore activity of hyperforin contributes to its pharmacological effects (Sell et al., 2014). These insights support the concept that activation of DAG-activated TRPC3 and TRPC6 channels are potential therapeutic approaches for neurological and psychiatric disorders. However, a framework for designing small molecule that activate DAG-activated TRPC channels, thus inducing neurotrophic effects on CNS, remains to be discovered.

In this study, we identified small molecule activators of DAG-activated TRPC3, TRPC6, and TRPC7 channels which showed trophic effects on neurons. Using a high-throughput screening assay, we identified nine piperazine derivatives by monitoring depolarizing effects on membrane potential in human embryonic kidney (HEK) cells expressing recombinant TRPC channels (Fig. 1B). Two piperazine compounds designated as PPZ1 ([4-(5-chloro-2-methylphenyl)piperazin-1-yl](3-fluorophenyl)methanone) and PPZ2 (2-[4-(2,3-dimethylphenyl)piperazin-1-yl]-N-(2-ethoxyphenyl)acetamide), potently activated TRPC3, TRPC6, and TRPC7 among TRPC subfamily and promoted neurite outgrowth and neuronal survival via downstream Ca^{2+}-dependent signals. These findings clearly support the potential of novel small molecule mimics of BDNF that target TRPC channels-dependent Ca^{2+} signaling as an important basis to develop leads

8

of therapeutic drugs for neurological and psychiatric disorders.

Materials and Methods

Synthesis of Piperazine Derivatives. The details of the synthesis of piperazine derivatives are provided in the Supplemental Data.

Reagents. Pyr3 and Pyr4 were synthesized as previously reported (Kiyonaka et al., 2009). Dimethyl sulfoxide (DMSO), SK&F 96365, ML-7, Tetrodotoxin, Nifedipine, Picrotoxin, Capsazepine, and Cyclosporine A were purchased from Sigma-Aldrich (St. Louis, MO). FLIPR® Membrane Potential (FMP) Assay Kit was from Molecular Devices (Sunnyvale CA). U73122, U73343, 1-oleoyl-2-acetyl-*sn*-glycerol (OAG) and KN-93 were from Calbiochem (Nottingham, UK). Recombinant human BDNF (248-BD) was from R&D systems (Minneapolis, MN). STO-609 was from Wako Pure Chemical Industries (Osaka, Japan). PD98059 was from Biomol (Plymouth Meeting, PA). Carbachol (CCh), fura-2 AM and BAPTA-AM were from Dojindo (Kumamoto, Japan). FK506 was from Fujisawa Pharmaceutical Co., Ltd. (Osaka, Japan).

Animals. Any procedures and protocols used for animal studies using rats were approved by the Institutional Animal Care and Use Committee of Kyoto University prior to the start of experiments. Two to six-day-old Wistar rat pups were purchased from Japan SLC (Shizuoka, Japan) with their mother. The rats were group-housed (8–10 pups with their mother) in a standard 12-hour light /12-hour dark cycle environment with water and food provided *ad libitum*. Any procedures and protocols used for animal studies with rabbits were approved by the Institutional Animal Care and Use Committee of Fukuoka University prior to the start of experiments. Japan white rabbits weighing 1.5–2.0 kg were purchased from Biotec (Tokyo, Japan)

10

cDNA Cloning and Recombinant Plasmid Construction. Plasmids of the pCI-neo vector carrying mouse TRPC1α, TRPC2, TRPC3, TRPC4β, TRPC5, TRPC6, and TRPC7 cDNA were used as previously described (Okada et al., 1999; Inoue et al., 2001; Yoshida et al., 2006; Kiyonaka et al., 2009). Plasmids of the pCI-neo vector carrying mouse TRPA1, TRPM2, rat TRPV1, and human TRPV4 cDNA were used as previously described (Hara et al., 2002; Yoshida et al., 2006; Takahashi et al., 2014). A pEF-BOS expression vector encoding human muscarinic type 1 receptor was provided by T. Haga (Gakushuin University, Tokyo, Japan).

Cell Culture and cDNA Expression. Human embryonic kidney (HEK) 293 cells (Boehringer Ingelheim, Ingelheim, Germany) were cultured in Dulbecco's modified Eagle's medium (DMEM) containing 10% fetal bovine serum, 30 units/ml penicillin, and 30 µg/ml streptomycin at 37°C under 95% air and 5% CO_2. HEK 293 cells were transfected with recombinant plasmids using SuperFect transfection reagent (Qiagen, Valencia, CA), according to the manufacturer's instruction. For measurements of $[Ca^{2+}]_i$ and TRPC currents, recombinant plasmids were co-transfected with pEGFP-F (Clontech Laboratories, Mountain View, CA) and pEGFP-N1 (Clontech Laboratories), respectively. HEK 293 cells harboring green fluorescence were used for analysis. Transfected cells were cultured for 36–48 hours prior to $[Ca^{2+}]_i$ measurement and electrophysiological measurements.

Generation of Stably TRPC6-Expressing Cell Clone. HEK 293 cells (Stratagene, La Jolla, CA) were transfected with a pCI-neo vector carrying mouse TRPC6 using

Lipofectamine® LTX transfection reagent (Invitrogen, Carlsbad, CA) according to the manufacturer's instructions.   For the selection of stably-transfected cell clones, cells were incubated in 10% FBS in Minimum Essential Eagle's Medium supplemented with G418 (400 μg/ml) and Blasticidin (5 μg/ml).   Among 219 cell clones, clone #112 was selected as the best based on its response to CCh.

Transfection of HEK 293 Cells for FLIPR® Membrane Potential Assay.   HEK 293 cells (Stratagene) were seeded at a density of 2.5×10^5 cells/well in 6-well plates. After overnight culture, HEK 293 cells were transfected with a plasmid of the pCI-neo vector carrying mouse TRPC3 using Lipofectamine® LTX for 4–6 hours at 37˚C according to the manufacturer's instructions.

FLIPR® Membrane Potential Screening Assay.   Chemical compound library, comprising 8,000 compounds purchased from ChemBridge (San Diego, CA), was screened for TRPC6 activators.   HEK 293 cells stably expressing TRPC6 (clone #112) were plated in 384-well black clear-bottom plates (Greiner Bio-one, Kremsmuenster, Austria) at a density of 5×10^3 cells/well.   After overnight culture, the culture medium were removed, and then cells were incubated with 20 μl of FMP probe diluted in Ca^{2+}-free 20 mM HEPES/Hank's Balanced Salt Solution for 1 hour at room temperature. Compounds diluted in Hank's Balanced Salt Solution were added at 10 μM (10 μl/well). Relative fluorescence intensities (530/595 nm; excitation/emission) were measured in a FLIPR® Tetra fluorometric imaging plate reader (Molecular Devices, Sunnyvale, CA) in 1 second interval for 140 seconds.   Following first round of screening, 315 positive compounds were further tested under the same protocol twice to verify reproducibility.

12

Next, 124 positive compounds were subjected to a further round of testing, in vector-transfected HEK 293 cells, designed to eliminate false positives. Finally, nine positive compounds were further characterized in vector- or TRPC3-transfected HEK 293 cells and HEK 293 cells stably expressing TRPC6, each in three independent experiments.

$[Ca^{2+}]_i$ Measurement. Transfected HEK 293 cells (Boehringer) were subjected to $[Ca^{2+}]_i$ measurement 3–16 hours after plating onto poly-L-lysine–coated glass coverslips. Fluorescence signals from fura-2 were measured in HEPES-buffered saline containing the following: 107 mM NaCl, 6 mM KCl, 1.2 mM $MgSO_4$, 2 mM $CaCl_2$, 11.5 mM glucose, and 20 mM HEPES (pH adjusted to 7.4 with NaOH). Fluorescence images of the cells were recorded and analyzed with the video image analysis system AQUACOSMOS (Hamamatsu Photonics, Shizuoka, Japan) according to the manufacturer's instructions. The 340:380-nm ratio images were obtained on a pixel-by-pixel basis and were converted to Ca^{2+} concentrations by in vivo calibration using 10 μM ionomycin (Calbiochem/EMD Chemicals, San Diego, CA) as described previously (Takahashi et al., 2008). For calculation of the EC_{50} value of PPZ1 and PPZ2 in TRPC3-, TRPC6-, and TRPC7-expressing HEK 293 cells, the plots were fitted to the Hill equation: $f(x) = A_0 + (A_{max} - A_0)/[1 + (EC_{50}/x)^n]$, where A_0 is the basal response, A_{max} is the maximum response, x is the PPZ1 or PPZ2 concentration, and n is Hill coefficient, using Kaleidagraph software (Synergy software, Reading, PA).

Preparation of Single Portal Vein Smooth Muscle Cells. Albino rabbits of either sexes weighing 1.5–2.0 kg (Biotec) were used. Each rabbit was anesthetized with an

13

intravenous injection of sodium pentobarbital (40 mg/kg) and butorphanol tartate (0.08 mg/kg) and killed quickly by exsanguination via the femoral artery. The abdominal cavity was opened and an approximately 1-cm-long segment of the portal vein was excised between the hepatic and splenic bifurcations. Connective tissues were removed with fine scissors and forceps and thin strips of portal vein smooth muscle, approximately 10 mm × 2 mm in length and width, were made and incubated successively in nominally Ca^{2+}-free Krebs solution and one containing 2 mg/ml collagenase type 3 (Worthington, Lakewood, NJ) at 36°C for 5 and 35–40 minutes, respectively. The collagenase-digested strips were then thoroughly rinsed and minced into small pieces in Ca^{2+}-free Krebs solution, and gently triturated with a large-bore, Pasteur pipette to disperse single cells. These cells were used for electrophysiological measurements within 3 hours after the dispersion.

Isolation, Culture, and Transfection of Rat Cerebellar Granule Neurons. Rat cerebellar granule neurons (CGNs) were prepared from 3 or 4 cerebella from 6 to 9-day-old Wistar rat pups (Japan SLC) as previously described (Uriu et al., 2010). Cells were plated on a polyethyleneimine-coated 13 mm circle glass, 3.5 cm-dish or 3.5-cm glass bottom dish at a density of 5×10^4 cells/cm^2 for reverse transcriptase-polymerase chain reaction (RT-PCR), neurite outgrowth measurement and western blotting and 2.5×10^5 cells/cm^2 for neuronal survival assay. Two to four hours after plating, the medium was changed to DMEM with 10% newborn calf serum, 26 mM KCl, 30 units/ml penicillin, and 30 µg/ml streptomycin. Cultures were maintained at 37°C in 95% air, 5% CO_2. Freshly isolated CGNs were transfected with 300 nM of siRNAs using the Rat Neuron Nucleofector® Kit (Lonza, Walkersville, MD) and G-13

14

program (Lonza) according to the manufacturer's instructions.   pEGFP-N1 (1 µg) was co-transfected as a transfection marker in neurite measurements and patch clamp recordings.   The siRNAs targeting rat TRPC3 (ON-TARGETplus SMARTPool, L-088687), TRPC6 (ON-TARGETplus SMARTPool, L-095094), and TRPC7 (ON-TARGETplus SMARTPool, L-090059) were purchased from Dharmacon (Lafayette, IN).   Non-targeting, randomized siRNA was synthesized and purified with the Silencer siRNA construction kit (Ambion, Foster City, CA).   The oligonucleotide sequence used for synthesis of non-targeting siRNA is 5'-GGGTATACTAGTGAATTAG-3' (forward), and 5'-CTAATTCACTAGTATACCC-3' (reverse).

Electrophysiology.   For whole-cell recording from transfected HEK 293 cells (Boehringer), coverslips with cells were placed in a chamber containing bath solutions. Macroscopic currents were recorded at room temperature using the whole-cell mode of the patch clamp technique with an EPC-10 amplifier (Heka Elektronik, Lambrecht/Pfalz, Germany) as described previously (Okada et al., 1999).   The patch electrodes prepared from borosilicate glass capillaries had a resistance of 2–4 MΩ were used in the recordings.   Current signals were filtered at 2.9 kHz with a 4-pole Bessel filter and digitized at 20 kHz.   Patchmaster (Heka Elektronik) software was used for command pulse control, data acquisition, and analysis.   Series resistance was compensated (by 50–70%) to minimize voltage errors.   Solutions had the following compositions, with the concentrations in mM unless otherwise indicated. Ca^{2+}-containing bath solution: 120 Na^+, 5 K^+, 1.2 Mg^{2+}, 1 Ca^{2+}, 129.4 Cl^-, 10 glucose, and 10 HEPES (pH 7.4 adjusted with NaOH, and osmolality adjusted to 300 mOsM with D-mannitol) and Ca^{2+}-free bath

15

solution: 120 Na^+, 5 K^+, 1.2 Mg^{2+}, 129.4 Cl^-, 1 EGTA, 10 glucose, and 10 HEPES (pH 7.4 adjusted with NaOH, and osmolality adjusted to 300 mOsM with D-mannitol); Cs^+ internal solution for whole-cell recording: 120 Cs^+, 2 Mg^{2+}, 4 Ca^{2+}, 32 Cl^-, 100 aspartate, 2 Na_2ATP, 10 BAPTA (1,2-bis(2-aminophenoxy)ethane-*N*,*N*,*N'*,*N'*-tetraacetic acid), 0.1 GTP, and 5 HEPES (pH 7.2 adjusted with CsOH, and osmolality adjusted to 290 mOsM with D-mannitol). For the recordings of whole-cell currents in HEK 293 cells, ramp pulses were applied every 5 seconds from –100 to +100 mV at a speed of 0.4 mV ms^{-1} after a 50-ms step to –100 mV from a holding potential of –60 mV.

For whole-cell recording from CGNs at 1–3 DIV and CGNs transfected with siRNA for 24–48 hours, macroscopic currents were recorded and analyzed with an EPC-10 amplifier (Heka Elektronik) and Patchmaster (Heka Elektronik) as described for HEK cells. The patch electrodes prepared from borosilicate glass capillaries had a resistance of 5–20 MΩ for CGNs were used in the recordings. Solutions had the following compositions, with the concentrations in mM unless otherwise indicated. Bath solution: 140 Na^+, 5 Tetraethylammonium$^+$, 1.2 Mg^{2+}, 1 Ca^{2+}, 149.4 Cl^-, 15 glucose, 10 HEPES, 0.001 tetrodotoxin, 0.1 picrotoxin, 0.01 nifedipine, and 0.03 Cd^{2+} (pH 7.4 adjusted with Tris, and osmolality adjusted to 300 mOsM with D-mannitol) (Zhang et al., 2008); Cs^+ internal solution: 120 Cs^+, 2 Mg^{2+}, 4 Ca^{2+}, 32 Cl^-, 100 aspartate, 2 Na_2ATP, 10 BAPTA, 0.1 GTP, and 5 HEPES (pH 7.2 adjusted with CsOH, and osmolality adjusted to 290 mOsM with D-mannitol). Bath solutions containing the same concentration of DMSO (0.3 %) with PPZ2-containing test solutions were used to record basal currents. The currents were continuously recorded at –60 mV and low-pass filtered at 500 Hz before analyses. To construct *I-V* relationship, ramp pulses

16

were applied from –100 to +100 mV at a speed of 0.4 mV ms^{-1} after a 50-ms step to –100 mV.

For current recording from rabbit portal vein smooth muscle cells, recording of whole-cell currents and data analysis were performed using a standard patch clamp system consisting of: an 'EPC-8' patch clamp amplifier: 'LIH8+8' DA, AD converter: Patchmaster v.1.1.2 (Heka Elektronik). The input resistance of electrodes used for whole-cell cell recording ranged from 8–15 MΩ, and 50–70% of access resistance (5–7 MΩ) was electronically compensated. For long-term recordings (> 1 minutes), the current signal was obtained using PowerLab 4/35 (digitized at 1 kHz; AD Instruments, Bella Vista, NSW) after low-pass filtering at 500 Hz from which the mean current amplitude were calculated over every 1 second segment. The liquid junction potential between pipette and bath solutions (–6 mV) was corrected when constructing current-voltage relationships. Test solutions were topically applied using the so-called 'Y-tube' fast solution exchange device which was controlled by one 3-way and two 2-way electromagnetic valves by DA outputs from the computer. Solutions had the following compositions, with the concentrations in mM unless otherwise indicated. Bath solution: 135 Na$^+$, 5 K$^+$, 1.2 Mg^{2+}, 1 Ca^{2+}, 151.4 Cl$^-$, 5 glucose, and 10 HEPES; and Cs$^+$ internal solution for whole-cell recording: 140 Cs$^+$, 2 Mg^{2+}, 24 Cl$^-$, 120 aspartate, 2 Na$_2$ATP, 5 phosphocreatine, 5 EGTA or BAPTA/1.5Ca^{2+}, 10 glucose and 10 HEPES. The composition of Ca^{2+}-free Krebs solution was, in mM; 140 Na$^+$, 6 K$^+$, 1.2 Mg^{2+}, 148.4 Cl$^-$, 10 glucose, and 10 HEPES (adjusted to pH 7.4 with Tris base). All experiments were performed at 24–26°C, either at ambient temperature or using a commercial warmer unit (TC-344B; Warner Instrument, Hamden, CT).

RT-PCR. Total RNA of cultured rat CGNs was extracted using ISOGEN following the manufacturer's instructions (Wako Pure Chemical Industries, Osaka, Japan). Reverse transcription of total RNA to cDNA was performed using the RNA LA PCR Kit (TaKaRa-Bio, Shiga, Japan). This cDNA was used as PCR template to detect genes expression using the following primers: TRPC1, 5'-GGTACATCTTCTCCTTAGCGC-3' (forward) and 5'-TGGTCTGTGCTCTGCATCTTC-3' (reverse); TRPC2, 5'-AGAAGCTGGGCAATTTCAACG-3' (forward) and 5'-CGATGAGCATGTTGAGTAGCACA-3' (reverse); TRPC3, 5'-TGAGGTGAACGAAGGTGAACTG-3' (forward) and 5'-CCTGTCCCCCAAGGAACTCT-3' (reverse); TRPC4, 5'-GCTTCGAAGTTCTGGGATTGC-3' (forward) and 5'-CACCACCACCTTCTCCGACTT-3' (reverse); TRPC5, 5'-CTAGCAGCGCTGAATTCTCTC-3' (forward) and 5'-AAGTTTCGAATTTGAGGAGCAGATG-3' (reverse); TRPC6, 5'-GGTTTACGGCAGCAGACCAT-3' (forward) and 5'-CGCATGTGCTACGAACTTCATG-3' (reverse); TRPC7, 5'-GAAGTACGACCACAAGTTCATCG-3' (forward) and 5'-TCAGGTGGTCTTTGTTCAAAT-3' (reverse); β-actin, 5'-TTCTACAATGAGCTGCGTGTGGC-3' (forward) and 5'-CTCATAGCTCTTCTCCAGGGAGGA-3' (reverse). PCR was conducted under the following conditions: 94°C for 2 minutes followed by 35 cycles for TRPC1–C7 or 20 cycles for β-actin of denaturation at 94°C for 30 seconds, annealing at 60°C for 30 seconds, and extension at 72°C for 1 minute, and finally 72°C for 7 minutes. Predicted

18

lengths of products were 477, 166, 469, 555, 502, 152, and 649 base pairs for TRPC1–C7 and 445 base pair (bp) for β-actin, respectively.

Measurement of Neurite Outgrowth in CGNs. Two to four hours after plating, neurons were stimulated with 0.1% DMSO, 50 ng/ml BDNF, PPZ1 or PPZ2 with or without various inhibitors for 24 hours. In experiments treating with siRNA, CGNs were stimulated with DMSO, 50 ng/ml BDNF, PPZ1 or PPZ2 at 24–48 hours after transfection for 24 hours. Neurons were fixed in phosphate buffer containing 4% paraformaldehyde/4% sucrose solution. Cells were permeabilized, and blocked with phosphate buffer containing 1% BSA/0.1% Triton X-100. Neurons were incubated overnight at 4°C with an anti-MAP2 antibody (M1406; 1:200, Sigma-Aldrich) in phosphate buffer and staining was detected by incubation with a secondary antibody, Alexa Fluor 488-conjugated goat anti-mouse IgG (A11017; 1:2000, Invitrogen) for 1 hour at room temperature. F-Actin were labeled for simultaneous detection by incubation with Alexa Fluor 546-phalloidin (A22283; 1:40, Invitrogen). Fluorescence images were acquired using a confocal laser-scanning microscope (IX71; Olympus, Tokyo, Japan) with FV500 software (Olympus). For analyses of total neurite length/cell, neurite lengths were measured by tracing neurites according to F-actin signals in each MAP2-positive cells using NeuronJ software (Meijering et al., 2004). Only neurites longer than one cell diameter were measured and values were averaged. Ten to twenty images from independent three experiments were used for the analyses.

Isolation, Culture and Neurite Measurements of Rat Hippocampal Neurons.
Primary hippocampal neurons were prepared from frozen hippocampus of 19-day

19

embryo Wistar rat (MBX0402; Sumitomo Bakelite, Tokyo, Japan) using Nerve Cell Dissociation Medium (MBX0802; Sumitomo Bakelite). The primary hippocampal neurons were plated onto a poly-D-lysine-coated 8 well chamber slides (BD Bioscience, San Jose, CA) at a density of 5×10^4 cells/well. The cultures were maintained at 37°C with 95% air and 5% CO_2. Four hours after plating, the medium was replaced with Neuron Assay Medium (MBX0701; Sumitomo Bakelite) containing 0.1% DMSO, 50 ng/ml BDNF, PPZ1 or PPZ2 with or without SK&F 96365, Pyr4, or capsazepine for 48 hours. Total neurite length/cell was determined by the same procedure with CGNs described above. Five to ten images from independent three experiments were used for the analyses.

Western Blotting. Two to four hours after plating, CGNs were stimulated with 0.1% DMSO or PPZ2 for indicated time. Then, CGNs were washed with PBS buffer and lysed with 300 μl of 1 × SDS sample buffer containing 50 mM dithiothreitol. Proteins from each lysate were separated by electrophoresis on a 10% SDS-polyacrylamide gel and then transferred onto immobilon-P membranes (Millipore, Billerica, MA). Phosphorylated and total CREB were detected by western blotting using an anti-phospho-CREB (Ser-133)-specific antibody (#9198; 1:1000, Cell signaling, Danvers MA) and an anti-CREB antibody (#9197; 1:1000, Cell signaling) as previously described (Chung et al, 2011), respectively, using the ECL system (Amersham Pharmacia Biotech, Piscataway, NJ). For loading normalization, α-tubulin was detected by using an anti-α-tubulin antibody (T6074; 1:2000, Sigma-Aldrich). The chemiluminescence intensities of the bands were measured by Multigauge version 3.0 (Fuji film, Tokyo, Japan). Ratios of phosphorylated CREB to total CREB,

reflecting CREB activation, were calculated from band intensities obtained in at least three independent experiments.

Cell Survival Assay.   Cell survival assays were performed as previously described (Jia et al., 2007) with minor modification.   Isolated CGNs were plated on 3.5-cm glass bottom dishes.   CGNs were pretreated with 0.1% DMSO, 50 ng/ml BDNF, PPZ1 or PPZ2 with or without 1 μM Pyr4 for 24 hours at 4 DIV, then medium was washed with DMEM containing 5 mM KCl without serum and incubated with this medium containing the pretreated agents for 24 hours to assess cell death.   Cell death was evaluated by Hoechst 33342 (Dojindo) and Propidium Iodide (PI) (Setareh Biotech, Eugene, OR) staining.   Cells were incubated with Hoechst 33342 (1 μg/ml) and PI (0.2 μg/ml) for 5 min at 37°C with 5% CO_2 to visualize nucleus and dead cells, respectively. Then, the staining was detected by using a fluorescence microscope (IX81; Olympus) with MetaMorph software (Molecular Devices).   Cell death ratio was calculated by dividing the number of PI positive cells by the number of nucleus, and shown as % PI positive cells.   Four to ten images containing at least 50 cells from at least three independent experiments were analyzed.

Statistical Analyses.   All data are expressed as means ± S.E.M.   In FMP assay, $[Ca^{2+}]_i$ measurements, electrophysiology, RT-PCR, Real-time PCR, neurite outgrowth measurements, western blot, survival assays, and luciferase assay, we accumulated the data for each condition from at least three independent experiments.   The statistical analyses were performed using the Student's t-test and a P value < 0.05 was considered significant.

21

Results

Screening of Novel Small Molecule Activators of DAG-Activated TRPC Channels

To search for small molecules that activate DAG-activated TRPC channels, we first carried out a high-throughput screening using a FMP assay in HEK 293 cells stably expressing TRPC6 (Fig. 2A). Fluorescence increases indicating membrane potential depolarization elicited by stimulation of endogenous muscarinic cholinergic receptors by CCh (Boulay et al., 1997; Kiyonaka et al., 2009) served as a positive control for TRPC6 channel activation (Fig. 2B). From a chemical library of 8000 compounds, we identified nine piperazine compounds, each eliciting a more than 20% increase in fluorescent intensity of the FMP probe in TRPC6-expressing cells (334.8 ± 95.0 a.u. for 30 μM compound 1 and 789.4 ± 15.5 a.u. for 30 μM compound 6) and not inducing significant changes in vector-transfected control cells. These nine piperazine compounds are categorized into two structural groups: five compounds contain a benzoyl or phenylsulfonyl piperazine structure (Compound A group) and four compounds contain a 1-phenyl piperazine-4-acetamide structure (Compound B group) (Fig. 1B). Further experiments with compounds 1 and 6 showed a gradual increase in membrane potential in not only TRPC6-expressing, but also TRPC3-expressing cells (Fig. 2, C and D). The compound groups A and B were examined for stimulation of TRPC3, TRPC6, and TRPC7, another DAG-activated cation channel, in $[Ca^{2+}]_i$ measurements. These compounds, each at 10 μM, evoked significant $[Ca^{2+}]_i$ increases in TRPC3-, TRPC6-, and TRPC7-expressing HEK 293 cells compared to vector-transfected HEK 293 cells (Fig. 2E). These results suggest that the nine identified piperazine compounds are a new series of activators of DAG-activated TRPC3, TRPC6, and TRPC7 channels. Among nine compounds, compound 6 had the

22

most potent effect on DAG-activated TRPC channels.   Notably, compound 6 at 10 μM

elicited robust $[Ca^{2+}]_i$ increase in TRPC6-expressing cells.

Characterization of the Compounds PPZ1 and PPZ2

For precise characterization, we focused on compound 1 and 6, which evoked

robust and comparatively similar responses of TRPC3/TRPC6/TRPC7 in measurements

conducted so far.   Compound 3 is similarly potent but has a bulky and lipophilic

benzyloxy group, which may limit optimization of the compound toward

pharmaceutical drugs.   Therefore, considering the smaller and simpler structure, we

selected compound 1 from group A (compound 1–5) for further investigation.   Because

both compounds share phenyl-piperazine structure, we designated them as PPZ1

(compound 1) and PPZ2 (compound 6), respectively.   PPZ1 (100 μM) and PPZ2 (30

μM) elicited significant $[Ca^{2+}]_i$ elevation in HEK 293 cells expressing TRPC3, TRPC6,

and TRPC7 but not in cells expressing TRPC1, TRPC2, TRPC4, and TRPC5 (Fig. 3, A

and B).   The data of PPZ1- and PPZ2-induced Ca^{2+} responses suggest activation

selectivity of the compounds PPZ1 and PPZ2 to TRPC3, TRPC6, and TRPC7 among

TRPC subfamily.   PPZ1 and PPZ2 evoked these Ca^{2+} signals in a

concentration-dependent manner (Fig. 3, C and D).   To estimate functional expression

levels of TRPC channels in HEK 293 cells, we have analyzed Ca^{2+} responses to 100 μM

CCh by the Ca^{2+} add-back protocol, which separates the $[Ca^{2+}]_i$ increase through Ca^{2+}

release from that through Ca^{2+} influx (Supplemental Fig. S1, A and B).   CCh-induced

Ca^{2+} influx is significantly higher in TRPC channel-transfected HEK 293 cells than

vector-transfected cells.   The maximum $[Ca^{2+}]_i$ rises elicited by 100 μM CCh are

comparable in TRPC3-, TRPC6-, and TRPC7-expressing HEK 293 cells, suggesting

that the levels of functional expression of these TRPC channels are similar in our system. The dose-response data was reanalyzed by normalizing the value of maximum $[Ca^{2+}]_i$ rise induced by PPZ compounds to those induced by adding back extracellular Ca^{2+} upon stimulation with 100 µM CCh, and the EC_{50} values were obtained by fitting the plots to the Hill equation (Supplemental Fig. S1, C and D). For TRPC3, TRPC6, and TRPC7, EC_{50} values of PPZ1 were 57.0, 67.3, and 45.9 µM and Hill coefficients were 0.80, 1.59, and 2.14, and EC_{50} values of PPZ2 were 10.20, 8.37, and 2.90 µM and Hill coefficients were 0.67, 1.67, and 1.25, respectively. Importantly, PPZ1- and PPZ2-induced Ca^{2+} responses were attributable mainly to Ca^{2+} influx through TRPC channels, because PPZ1 and PPZ2 failed to evoke significant $[Ca^{2+}]_i$ elevation in Ca^{2+}-free extracellular solutions (Supplemental Fig. S2, A–D). We also examined the effects of PPZ1 and PPZ2 on CCh-induced activity of TRPC3, TRPC6, and TRPC7 in $[Ca^{2+}]_i$ measurements. Ten µM PPZ2 enhanced CCh-induced Ca^{2+} influx in TRPC6 and TRPC7-expressing HEK 293 cells, but 10 µM PPZ1 and 30 µM 1-oleoyl-2-acetyl-sn-glycerol (OAG), a membrane-permeable DAG-analogue, failed to exert such effects (Supplemental Fig. S3, A and B). This result suggests that PPZ2 may activate TRPC6 and TRPC7 in part via a mechanism not induced by receptor stimulation.

PPZ1 and PPZ2 were further examined for their effects on TRPM2, TRPA1, and TRPV1 using $[Ca^{2+}]_i$ measurements and for TRPV4 by whole-cell patch clamp recordings (Supplemental Fig. S4). PPZ1 had no significant effects on TRPM2, TRPA1, or TPRV4, while it activated TRPV1 at 10–100 µM. PPZ2 had no significant effects on TRPM2 and TRPV4, while it activated TRPA1 and TRPV1 at 30 µM, a markedly higher concentration than those needed to activate TRPC3, TRPC6, and

TRPC7.   Thus,   the   obtained   results   suggest   that   PPZ2   selectively   targets DAG-activated TRPC channels at concentrations as high as 10 μM, in contrast to PPZ1, which efficiently activates TRPV1 as well at 10 μM.

Both PPZ1 and PPZ2, in the external solution also containing the PLC inhibitor U73122 (Bleasdale et al., 1990), still induced $[Ca^{2+}]_i$ increases in TRPC3-, TRPC6-, and TRPC7-expressing cells (Fig. 3, E–H).   This indicated that the Ca^{2+} responses induced by PPZ1 and PPZ2 are not due to an indirect activation of these channels via the PLC pathway.

In whole-cell patch clamp recordings, PPZ1 and PPZ2 increased whole-cell currents in HEK 293 cells expressing TRPC3, TRPC6, or TRPC7 but not in control cells (Fig. 4, A–D).   Current-voltage (*I-V*) relationships of the currents in TRPC3-, TRPC6-, or TRPC7-expressing cells showed prominent rectification at depolarizing potentials, consistent with previous reports for receptor-operated TRPC3, TRPC6, or TRPC7 currents (Hofmann et al., 1999; Okada et al., 1999).   We then, tested the extracellular Ca^{2+}-dependence of PPZ1- and PPZ2-induced currents in TRPC6-expressing HEK 293 cells.   TRPC6 currents induced by 100 μM PPZ1, 30 μM PPZ2, and 100 μM CCh in the absence of extracellular Ca^{2+} were suppressed by addition of 1 mM extracellular Ca^{2+} (Supplemental Fig. S5).   This result suggests that extracellular Ca^{2+} is not an obligatory necessity but can act as a modulator in PPZ1- and PPZ2-induced TRPC6 activation as in receptor-induced TRPC6 activation.

We further examined PPZ2-induced TRPC6 channel activity by a cell-attached configuration in TRPC6-transfected HEK 293 cells.   Application of PPZ2 from pipette significantly increased ion channel activity with a mean NP_o (the product of the number of channels (N) and the channel open probability (P_o)) value from 0.0093 ± 0.0083

(DMSO) to 0.070 ± 0.032 (PPZ2, $p < 0.05$), which was not observed in vector-transfected HEK 293 cells (0.0055 ± 0.0030, $p < 0.05$ compared to TRPC6-transfected cells) (Supplemental Fig. S6, A and B). PPZ2 induced TRPC6 currents which opened to multiple unitary current amplitude levels, comparable to the TRPC6 currents observed in mesenteric artery myocytes (Saleh et al., 2006). Other than a unitary current which had a smaller single channel conductance (15.8 pS), we found a larger unitary current amplitude with a conductance of 30.4 pS (calculated from the inward portion of *I-V* relationship) almost identical to that of receptor-activated recombinant TRPC6 currents in previous reports (Hofmann et al., 1999; Shi et al., 2004) (Supplemental Fig. S6C). The amplitude of the unitary current with the conductance of 30.4 pS was 2.1 pA in the presence of PPZ2 at –60 mV, being similar to 2.0 pA of the unitary current observed in the absence of PPZ2. These results may suggest that PPZ2 triggers activation gating or stabilizes the open state of TRPC6 channel without affecting the ion permeability of the opened channel, at least in part through a mechanism shared by physiological receptor stimulation.

PPZ2, in a concentration dependent manner, also induced whole-cell currents in isolated rabbit portal vein smooth muscle cells (Fig. 5, A–C), in which TRPC6 was reported to play a predominant role in receptor-operated cation influx (Inoue et al., 2001). Ten µM noradrenaline (Norad) was used as a positive control to induce non-selective cation currents through TRPC6. Since TRPV1 is also expressed in smooth muscle cells (Mori et al., 2015), it may contribute to ionic currents induced by PPZ2 at 30 µM in rabbit portal vein smooth muscle cells according to our results (Supplemental Fig. S4C). However, PPZ2 at 1 and 3 µM, which are subthreshold concentrations to activate TRPV1 channels, enhanced the ionic currents in rabbit portal

26

vein smooth muscle cells. This supports that we were able to isolate native TRPC6 currents activated by PPZ2 in rabbit portal vein smooth muscle cells.

Piperazine Compounds PPZ1 and PPZ2 Promote Neurite Outgrowth via TRPC3, TRPC6 and TRPC7 Channels

TRPC3 and TRPC6 are reportedly involved in neuronal development such as neurite outgrowth and dendritic morphological changes (Li et al., 2005; Amaral and Pozzo-Miller, 2007; Tai et al., 2008). Therefore, to investigate whether the PPZ compounds have such pharmacological effects, we isolated rat cerebellar granule neurons (CGNs), which endogenously express TRPC channels as confirmed by RT-PCR and real-time PCR (Fig. 6A; Supplemental Fig. S7). CGNs treated with PPZ1 and PPZ2 (3–300 nM) had significantly greater neurite outgrowth, measured by total neurite length, as compared with control CGNs treated with vehicle (DMSO) (Fig. 6, B and C). Promotion of neurite outgrowth by both compounds was suppressed by Pyr3, the selective TRPC3 inhibitor or by Pyr4, which inhibits TRPC3, TRPC6, and TRPC7 (Kiyonaka et al., 2009) (Fig. 6D). It was also inhibited by a mixture of specific siRNAs for TRPC3, TRPC6, and TRPC7 (siTRPC3/6/7), each of which efficiently suppressed expression (Fig. 6, E and F). These data suggest that PPZ1 and PPZ2 promote neurite outgrowth through activation of endogenous TRPC3, TRPC6, and TRPC7 in CGNs.

We tested the effects of co-treatment of PPZ1 or PPZ2 at various concentrations (0.01–10 μM) with BDNF in neurite outgrowth assay (Supplemental Fig. S8A). PPZ2 at relatively high concentrations ($\geq$ 1 μM) but not PPZ1 (0.01–10 μM) suppressed promotion of neurite outgrowth induced by BDNF. To address the underlying

mechanisms of suppressive effects of PPZ2 on BDNF-induced neurite outgrowth, we assessed cell toxicity induced by PPZ1 or PPZ2 by itself. PPZ2 but not PPZ1 increased neuronal apoptosis at high concentrations (10 and 30 μM) (Supplemental Fig. S8B). This was rescued by co-treatment of the membrane-permeable Ca^{2+} chelator BAPTA-AM (Supplemental Fig. S8C). These results may suggest that PPZ2 at high concentrations induces Ca^{2+} overload in CGNs, leading to induction of cell death and suppression of BDNF-induced neurite outgrowth. This is consistent with the observation that PPZs applied alone lack promoting effects at relatively high concentrations on neurite growth (Fig. 6C), and interestingly contrasts with the promoting effect of PPZs at relatively low concentrations on neurite outgrowth (Fig. 6, C and D) and neuronal survival (See the data in the last part of the Results section).

PPZ1 and PPZ2 also promoted neurite outgrowth in isolated rat hippocampal neurons, in which DAG-activated TRPC channels were endogenously expressed, as shown by real-time PCR, but TRPV1 was poorly expressed (Supplemental Fig. S7). PPZ1- and PPZ2-induced neurite outgrowth was suppressed by 1 or 20 μM SK&F 96365 (SKF), a non-selective inhibitor for various cation and Ca^{2+} influx channels including TRPC channels (Merritt et al., 1990) and 1 μM Pyr4, but not by 0.1 μM capsazepine (CPZ), a TRPV1 inhibitor (Dickenson and Dray, 1991) (Fig. 6, G and H, Supplemental Fig. S9). These results support the growth-promoting effects of the PPZ compounds PPZ1 and PPZ2 in neurons, endogenously expressing TRPC3, TRPC6, or TRPC7.

We examined activation of endogenous DAG-activated TRPC channels by PPZ2 in whole-cell mode of patch clamp recordings in CGNs. Application of PPZ2 induced inward currents which showed TRPC3/TRPC6/TRPC7-like *I-V* relationships (Fig. 7

A–D: compare with recombinant currents in Fig. 4), and knockdown of TRPC3, TRPC6, and TRPC7 using mixture of specific siRNAs (siTRPC3/6/7: Fig. 6, E and F) nearly abolished PPZ2-induced currents in CGNs (Fig. 7, E and F).   These results support that PPZ2 activates endogenous DAG-activated TRPC channels in CGNs.

Neurite Outgrowth is Promoted by Piperazine Compounds via Ca^{2+}-Dependent Signaling Pathways

Ca^{2+} signaling initiated by TRPC3 and TRPC6 plays multiple roles in physiological functions in neurons (Abramowitz and Birnbaumer, 2009; Nilius and Szallasi, 2014; Feng et al., 2015).   We sought to clarify how Ca^{2+} signaling pathways are involved in the biological effects of PPZ compounds in neurons.   In cultured rat CGNs, PPZ2 induced $[Ca^{2+}]_i$ increases (Fig. 8, A–C).   These Ca^{2+} responses were predominantly attributable to Ca^{2+} influx, because, in the absence of extracellular Ca^{2+}, PPZ2 caused only a marginal $[Ca^{2+}]_i$ increases in CGNs.   Next, we tested various pharmacological inhibitors of Ca^{2+}-dependent signaling, which suppressed BDNF-induced neurite outgrowth promotion in CGNs (Fig. 8D).   SK&F 96365 (SKF, 20 μM), the myosin light chain kinase (MLCK) inhibitor ML-7 (10 μM), the CaMK kinase (CaMKK) inhibitor STO-609 (STO, 5 μM), the CaMKII inhibitor KN-93 (2 μM), and the MAPK/ERK kinase (MEK) inhibitor PD98059 (PD, 50 μM) significantly suppressed the promoting effects of PPZ1 and PPZ2 on neurite outgrowth in CGNs.   In contrast, the calcineurin inhibitors cyclosporine A (CsA, 10 μM) and FK506 (1 μM) failed to suppress the PPZ1 and PPZ2 effects.   To confirm the suppressive activity of these inhibitors on calcineurin, we tested their effects on the activity of the main downstream signaling molecule of calcineurin, nuclear factor of activated T-cells

(NFAT), using luciferase reporter vector which contains NFAT binding sequences in CGNs (Supplemental Fig. S10). BDNF significantly increased NFAT activity in CGNs, as previously reported (Groth and Mermelstein, 2003). By contrast, 10 nM PPZ1 and PPZ2 failed to show this effect. Ten μM CsA and 1 μM FK506 nearly abolished the constitutive NFAT activity, which was slightly rescued by BDNF. These results indicate that the calcineurin/NFAT pathway is induced in our experimental condition, further supporting the notion that the calcineurin/NFAT pathway is not involved in PPZ-induced neurite outgrowth.

CaMKK, CaMKII and MEK are known to activate Ca^{2+}-dependent transcription factor CREB in response to $[Ca^{2+}]_i$ increases (Shaywitz and Greenberg, 1999). Indeed, treatment with PPZ2 significantly increased CREB Ser-133 phosphorylation in CGNs (Fig. 8, E and F). This result is consistent with a previous report demonstrating the importance of TRPC3 and TRPC6 in BDNF-induced activation of MAPK, CaMK, and the downstream molecule CREB (Jia et al., 2007). ML-7 decreases growth cone motility via inhibition of MLCK (Ruchhoeft and Harris, 1997), the Ca^{2+}-dependent actin filament modulator. PPZ compounds therefore may also affect the cytoskeleton during neurite outgrowth through MLCK. Thus, PPZ1 and PPZ2 promote neurite outgrowth of CGNs by triggering Ca^{2+}-dependent signaling pathways essential for modulation of gene expression and actin dynamics.

Piperazine Compounds PPZ1 and PPZ2 Promote Neuronal Survival through TRPC3, TRPC6 and TRPC7 Channels

BDNF-induced TRPC3 and TRPC6-dependent CREB activation is known to promote neuronal survival in CGNs (Jia et al., 2007). As described above, our data

indicates that PPZ2 induces activation of CREB. Therefore, we tested neuroprotective effects of the PPZ compounds in cultured CGNs subjected to serum deprivation-induced cell death. This is also an important experiment to know the biological activity of PPZ2 at concentrations in the context of neuronal death/survival. When CGNs were pretreated for 24 hours before serum deprivation and incubated also during serum deprivation (24 hours) with the compounds PPZ1 and PPZ2, CGNs showed significantly reduced cell death, indicated by the marker propidium iodide (PI), as compared with DMSO-treated control CGNs (Fig. 9, A and B). PPZ1 was effective at concentrations of 100 and 1,000 nM, while PPZ2 was at 1 and 10 nM, in contrast to PPZ2 at higher concentrations (10 and 30 μM) required in inducing cell death. Co-administration of Pyr4 (1 μM) with BDNF, PPZ1, or PPZ2 reversed the percentage of PI positive cells to the level as with the DMSO-treated control (Fig. 9C). These results show that PPZ1 and PPZ2, like BDNF, promote survival of CGNs.

Taken together, our findings suggest that the PPZ compounds PPZ1 and PPZ2 activate DAG-activated TRPC3, TRPC6, and TRPC7 channels, and stimulate Ca^{2+}-dependent signaling pathways, leading to trophic effects such as promotion of neurite outgrowth and survival in neurons.

Discussion

We have identified novel small molecule, piperazine-derived activators of DAG-activated TRPC channels as a new class of BDNF mimetics. More specifically, PPZ1 and PPZ2 selectively activate, among TRPC subfamily members, TRPC3/C6/C7, thereby promoting neurite outgrowth and survival in isolated rat neurons. We hypothesize that activation of Ca^{2+}-dependent signaling by Ca^{2+} influx via TRPC3/C6/C7 mediates the neurotrophic action of the PPZs.

The nine low-molecular-weight small compounds identified by our chemical library screening all have a piperazine scaffold, and fall into two groups. Group A comprises benzoyl-piperazines (compound 1–4) and sulfonyl piperazines (compound 5) and Group B comprises 1-phenyl-piperazine-4-aceto amide derivatives (compound 6–9) (Fig. 1B). Though our screening was based on TRPC6 activation, subsequent experiments revealed that the selected compounds also activated the closely related TRPC subtypes, TRPC3 and TRPC7. DAG and its analogue OAG (Fig. 1A), originally used as potent activators of PKCs (Nishizuka, 1995), activate TRPC3/C6/C7 (Hofmann et al., 1999; Okada et al., 1999). Though further studies are needed to clarify the mechanism of action, it is important that PPZs selectively activate DAG-activated TRPC channels without directly affecting PKCs. Because PKCs directly phosphorylate various signaling proteins including TRPC3/C6/C7 to control intracellular signal transduction upon PLC-coupled receptor stimulation or OAG application (Okada et al., 1999; Venkatachalam et al., 2003; Bousquet et al., 2010; Numaga et al., 2010), PPZs would activate particular pathways more selectively than PLC-coupled receptor stimulation or OAG. In $[Ca^{2+}]_i$ measurements and patch clamp recordings, the compounds PPZ1 and PPZ2 failed to activate other TRPCs, TRPM2, or

TRPV4. PPZ1 also activated TRPV1 at 10 μM, while PPZ2 activated TRPV1 and TRPA1 only at 30 μM, a concentration markedly higher than those needed to activate TRPC3/C6/C7. Based only on the obtained data so far, we cannot exclude the possibility that PPZ1 and PPZ2 affect other channels, receptors or intracellular molecules. However, PLC inhibition failed to affect PPZ1- and PPZ2-induced TRPC activation, suggesting that involvements of PLC pathways are unlikely possibility. Moreover, immediate action of the compounds in whole-cell recordings is consistent with a direct action of PPZs on the channels. Although our cell-attached recordings suggest that PPZ2-induced TRPC6 currents share functional properties with receptor-activated TRPC6 currents, $[Ca^{2+}]_i$ measurements showed that PPZ2 further enhances TRPC6 and TRPC7 activity elicited under CCh stimulation, suggesting a mechanism different from receptor stimulation in the activation of TRPC6 and TRPC7 by PPZ2. Further evaluations will be required to demonstrate mechanisms of selective action of the PPZs on DAG-activated TRPC channels.

PPZ1 and PPZ2 dose-dependently activate TRPC3/C6/C7. Though we could not obtain complete dose-response relationship data due to poor water solubility, by fitting the plots to the Hill equation, we obtained the EC_{50} values, which reveal that PPZ2 has higher affinities to DAG-activated TRPC channels than PPZ1. Interestingly, both compounds showed the lowest EC_{50} values to TRPC7. Moreover, the nine compounds identified in our screening activated TRPC7 at high potencies. Therefore, our compounds are potential new leads to develop selective activators of TRPC7, providing useful tools to investigate the physiological and pharmacological significance of TRPC7, the most elusive TRPC channel.

PPZ1 and PPZ2 promoted neurite outgrowth and survival in CGNs. Inhibition

or downregulation of TRPC3/C6/C7 suppressed these beneficial effects. PPZ-induced neurite outgrowth was suppressed by inhibitors of MLCK, CaMKK, CaMKII, and MEK, all of which are activated by $[Ca^{2+}]_i$ increases (Kamm and Stull, 2001; Agell et al., 2002; Wayman et al., 2008). This, together with the observations that PPZ2 induced TRPC3/C6/C7-like currents and $[Ca^{2+}]_i$ increases in CGNs, suggests that Ca^{2+}-induced signaling pathways via TRPC is of pivotal importance for neurotrophic effects of PPZs.

MLCK is an important regulator of growth cone motility through Ca^{2+}-dependent modulation of actin dynamics (Ruchhoeft and Harris, 1997; Zheng and Poo, 2007). Therefore, PPZ-induced MLCK activation via $[Ca^{2+}]_i$ increase may affect growth cone motility. This idea is consistent with essential roles of TRPC3 and TRPC6 in BDNF-induced growth cone turning (Li et al., 2005). In addition to MLCK, PPZ2-induced $[Ca^{2+}]_i$ increases stimulate CaMKK, CaMKII and MEK, components of CaMK and MAPK pathways. Because PPZ2 promoted CREB activation in CGNs, Ca^{2+}-dependent activation of these pathways by PPZ2 is likely to converge at CREB activation, thus leading to the neurotrophic actions of PPZ2 (Shaywitz and Greenberg, 1999). This is supported by the previous findings that TRPC3 and TRPC6 mediate Ca^{2+}-dependent activation of CaMK, MAPK, and CREB in neurons (Jia et al., 2007; Tai et al., 2008; Heiser et al., 2013).

Our data fail to reveal roles of calcineurin in PPZ-induced neurite outgrowth, though important roles have been previously suggested for calcineurin and its downstream transcription factor NFAT in neurite outgrowth and survival induced by neurotrophins (Graef et al., 2003; Benedito et al., 2005). Importantly, other than TRPC-dependent pathways, BDNF induces Ca^{2+} release from ER and Ca^{2+}-independent activation of MAPK-ERK and phosphatidylinositol 3-kinase-Akt pathways to induce

neurotrophic effects (Huang and Reichardt, 2003). This was apparent in neurite growth, when TRPC3/C6/C7 were fully blocked by SK&F 96365 or Pyr4 in hippocampal neurons (Fig 6H). In BDNF-induced calcineurin activation, $[Ca^{2+}]_i$ increase via Ca^{2+} release has a primary role (Nguyen and Di Giovanni, 2008). In contrast, PPZ1 and PPZ2 failed to induce Ca^{2+} release in HEK 293 cells or evoked only marginal Ca^{2+} release in CGNs (Fig. 8, A–C; Supplemental Fig. S2). Moreover, BDNF but not 10 nM PPZ1 nor PPZ2 activated NFAT (Supplemental Fig. S10). These results altogether suggest that PPZ1 and PPZ2 activate a part of the pathways of BDNF, to partially mimic its neurotrophic effect. Importantly, only "recombinantly overexpressed" TRPC6 has been reported to activate the calcineurin pathway without cellular stimulation in cultured hippocampal neurons (Shen et al., 2013). In the calcineurin-mediated pathway, previous reports have studied roles of endogenous TRPC3/C6/C7 activation upon receptor stimulation, which induces Ca^{2+} release (Onohara et al., 2006; Kiyonaka et al., 2009), but not roles of endogenous TRPC3/C6/C7 "directly" acivated.

An aberrant elevation of calcineurin/NFAT signaling is associated with numerous deleterious processes linked to neurodegenerative disorders such as synaptic dysfunction, neuritic atrophy, and neuronal death (Wu et al., 2010). Also, TRPC3 and TRPC6 have been implicated in cardiac hypertrophy through activation of calcineurin and NFAT (Onohara et al., 2006; Kiyonaka et al., 2009). Considering the lack of effect of PPZ1 and PPZ2 on the calcineurin/NFAT pathway, PPZ1 and PPZ2 may have a merit to evade undesired side effects induced through activation of calcineurin/NFAT signaling in the brain and the heart. These considerations may suggest that PPZ1 and PPZ2 have the potential to become leading compounds for development of new drugs

35

for neurodegenerative disorders.

CGNs mainly express TRPC6, while hippocampal neurons express TRPC3/C6/C7 at almost the same and much higher level than CGNs, which may allow PPZ1 (0.1 and 1 μM) to show potency of neurite outgrowth higher in hippocampal neurons than in CGNs.   By contrast, PPZ2 showed similar potency in these neurons. Interestingly, at relatively low concentrations (1 μM), PPZ2 preferentially activates TRPC7, while PPZ1 activates TRPC3 and TRPC7 (Fig. 3, C and D), suggesting that TRPC3 may contribute to the robust effect of PPZ1 in hippocampal neurons.   In hippocampal neurons and CGNs, TRPV1, which is activated by PPZ1, is only marginally expressed, compared to TRPC3/C6/C7.   Furthermore, capsazepine failed to affect PPZ1- and PPZ2-induced neurite growth promotion in hippocampal neurons. These results suggest that TRPV1 is not involved in PPZ-induced promotion of neurite outgrowth in CGNs and hippocampal neurons (Fig. 6H).   Although we cannot completely exclude the possibility of off-target effects of PPZ1, TRPV1 is unlikely the main pathway in robust PPZ1-induced hippocampal neurite outgrowth.

High concentrations of PPZ2 showed neuronal toxicity which was rescued by BAPTA-AM in CGNs, suggesting that Ca^{2+} overload due to excessive activation of TRPC channels underlies the suppressive effects of PPZ2 at high concentrations. PPZ1 at 100 μM induced prominent Ca^{2+} responses and ionic currents (poor solubility precluded us from testing 100 μM PPZ2).   However, PPZ2 showed higher efficacy than PPZ1 up to 30 μM in terms of Ca^{2+} responses and membrane depolarization (Fig. 2 and 3, and Supplemental Fig. S1).   Also, PPZ2 (>1 μM) but not PPZ1 (1–30 μM) induced cell death (Supplemental Fig. S8).   Taken together, PPZ2 has stronger effects to enhance TRPC activity than PPZ1.   This may enable PPZ2 to exert neurotrophic

36

effects at low concentrations, but deleterious effects on neurons via Ca^{2+} overload and maybe Na^+ overload at high concentrations.

PPZ1 and PPZ2 induced neurotrophic effects at concentrations lower than those required to activate recombinant TRPCs. This difference implies enhancements of PPZ-induced signaling in native preparations. It has been reported that TRPC3 and TRPC6 activation leads to membrane depolarization that activates voltage-dependent Ca^{2+} channels in excitable cells (Reading et al., 2005; Onohara et al., 2006; Qu et al., 2012). In CGNs, 30 μM PPZ2 evoked spike-like $[Ca^{2+}]_i$ increases that are abolished by depriving external Ca^{2+}. This robust Ca^{2+} response may be due to voltage-dependent Ca^{2+} channel activation following cation influx through TRPCs, a possible explanation for enhancement of the PPZ-induced signaling. Our results also suggest that PPZ-induced Ca^{2+} influx via TRPCs activates CREB, which regulates expression of BDNF (Tao et al., 1998). It is possible that TRPC3-mediated $[Ca^{2+}]_i$ increases promote BDNF release (Vohra et al., 2013) to enhance PPZ-induced neurotrophic effects. Interestingly, hyperforin and its analogue 2,4-diacylphloroglucinol, Hyp9 (Fig. 1A), activate only TRPC6 but still promote neurite outgrowth and dendritic morphological changes (Leuner et al., 2007; Leuner et al., 2010; Heiser et al., 2013). However, not only TRPC6 but TRPC3 plays important roles in neuronal functions such as chemoattraction, neurotransmitter release, synaptic plasticity, and neuronal survival (Li et al., 2005; Jia et al., 2007; Amaral and Pozzo-Miller, 2007; Hartmann et al., 2008). This leads us to postulate a synergy between PPZ-induced activation of TRPC3 and TRPC6 and their ability to promote neurotrophic effects at nanomolar concentrations.

In conclusion, we have identified novel PPZ activators of TRPC3/C6/C7, thereby identifying a novel pharmacophore for these TRPCs. PPZs exert potent neurotrophic effects by inducing Ca^{2+}-dependent signaling via TRPC3/C6/C7. It is important to note that PPZs, especially PPZ1 and PPZ2, are different in number of aspects of their activity, including TRP subtype selectivity. This suggests that there is still a room for improvement on affinity/selectivity to DAG-activated TRPCs to enhance the BDNF-like effect of PPZs. Further structural optimization and *in vivo* experiments are necessary to eventually allow PPZ compounds to become leads in the development of BDNF-mimetic TRPC activators.

Authorship Contributions

Participated in research design: Sawamura, Kawamura, Tanikawa, Kiyonaka, Mori MX, Nagata, Mori Y.

Conducted experiments: Sawamura, Hatano, Takada, Hino, Kawamura, Tanikawa, Nakagawa, Hase, Nakao, Hirano, Rotrattanadumrong, Hu, Inoue.

Performed data analysis: Sawamura, Hatano, Takada, Hino, Nakagawa, Mori MX, Inoue.

Wrote or contributed to the writing of the manuscript: Sawamura, Takada, Nakagawa, Kiyonaka, Mori MX, Nishida, Inoue, Mori Y.

References

Abramowitz J and Birnbaumer L (2009) Physiology and pathophysiology of canonical transient receptor potential channels. *FASEB J* **23**:297–328.

Agell N, Bachs O, Rocamora N and Villalonga P (2002) Modulation of the Ras/Raf/MEK/ERK pathway by Ca^{2+}, and calmodulin. *Cell Signal* **14**:649–654.

Amaral MD and Pozzo-Miller L (2007) TRPC3 channels are necessary for brain-derived neurotrophic factor to activate a nonselective cationic current and to induce dendritic spine formation. *J Neurosci* **27**:5179–5189.

Autry AE and Monteggia LM (2012) Brain-derived neurotrophic factor and neuropsychiatric disorders. *Pharmacol Rev* **64**:238–258.

Benedito AB, Lehtinen M, Massol R, Lopes UG, Kirchhausen T, Rao A and Bonni A (2005) The transcription factor NFAT3 mediates neuronal survival. *J Biol Chem* **280**:2818–2825.

Bleasdale JE, Thakur NR, Gremban RS, Bundy GL, Fitzpatrick FA, Smith RJ and Bunting S (1990) Selective inhibition of receptor-coupled phospholipase C-dependent processes in human platelets and polymorphonuclear neutrophils. *J Pharmacol Exp Ther* **255**:756–768.

Boulay G, Zhu X, Peyton M, Jiang M, Hurst R, Stefani E and Birnbaumer L (1997) Cloning and expression of a novel mammalian homolog of Drosophila transient receptor potential (Trp) involved in calcium entry secondary to activation of receptors coupled by the Gq class of G protein. *J Biol Chem* **272**:29672–29680.

Bousquet SM, Monet M and Boulay G (2010) Protein kinase C-dependent phosphorylation of transient receptor potential canonical 6 (TRPC6) on serine 448 causes channel inhibition. *J Biol Chem* **285**:40534–40543.

Chung YH, Sun Ahn H, Kim D, Hoon Shin D, Su Kim S, Yong Kim K, Bok Lee W and Ik Cha C (2006) Immunohistochemical study on the distribution of TRPC channels in the rat hippocampus. *Brain Res* **1085**:132–137.

Chung YW, Kim HK, Kim IY, Yim MB and Chock PB (2011) Dual function of protein kinase C (PKC) in 12-O-tetradecanoylphorbol-13-acetate (TPA)-induced manganese superoxide dismutase (MnSOD) expression: activation of CREB and FOXO3a by PKC-α phosphorylation and by PKC-mediated inactivation of Akt, respectively. *J Biol Chem* **286**:29681–29690.

Clapham DE (2003) TRP channels as cellular sensors. *Nature* **426**:517–524.

Clapham DE, Julius D, Montell C and Schultz G (2005) International Union of Pharmacology. XLIX. Nomenclature and structure-function relationships of transient receptor potential channels. *Pharmacol Rev* **57**:427–450.

Dickenson AH and Dray A (1991) Selective antagonism of capsaicin by capsazepine: evidence for a spinal receptor site in capsaicin-induced antinociception. *Br J Pharmacol* **104**:1045–1049.

Feng S, He Z, Li H and Wang Y (2015) Ca^{2+} signaling initiated by canonical transient receptor potential channels in dendritic development. *Neurosci Bull* **31**: 351–356.

Graef IA, Wang F, Charron F, Chen L, Neilson J, Tessier-Lavigne M and Crabtree GR (2003) Neurotrophins and netrins require calcineurin/NFAT signaling to stimulate outgrowth of embryonic axons. *Cell* **113**:657–670.

Griesi-Oliveira K, Acab A, Gupta AR, Sunaga DY, Chailangkarn T, Nicol X, Nunez Y, Walker MF, Murdoch JD, Sanders SJ, Fernandez TV, Ji W, Lifton RP, Vadasz E, Dietrich A, Pradhan D, Song H, Ming GL, Gu X, Haddad G, Marchetto MC,

Spitzer N, Passos-Bueno MR, State MW and Muotri AR (2014) Modeling non-syndromic autism and the impact of TRPC6 disruption in human neurons. *Mol Psychiatry* **20**:1350–65.

Groth RD and Mermelstein PG (2003) Brain-derived neurotrophic factor activation of NFAT (nuclear factor of activated T-cells)-dependent transcription: a role for the transcription factor NFATc4 in neurotrophin-mediated gene expression. *J Neurosci* **23**:8125–8134.

Hara Y, Wakamori M, Ishii M, Maeno E, Nishida M, Yoshida T, Yamada H, Shimizu S, Mori E, Kudoh J, Shimizu N, Kurose H, Okada Y, Imoto K and Mori Y (2002) LTRPC2 Ca^{2+}-permeable channel activated by changes in redox status confers susceptibility to cell death. *Mol Cell* **9**:163–173.

Hartmann J, Dragicevic E, Adelsberger H, Henning HA, Sumser M, Abramowitz J, Blum R, Dietrich A, Freichel M, Flockerzi V, Birnbaumer L and Konnerth A (2008) TRPC3 channels are required for synaptic transmission and motor coordination. *Neuron* **59**:392–398.

Heiser JH, Schuwald AM, Sillani G, Ye L, Muller WE and Leuner K (2013) TRPC6 channel-mediated neurite outgrowth in PC12 cells and hippocampal neurons involves activation of RAS/MEK/ERK, PI3K, and CAMKIV signaling. *J Neurochem* **127**:303–313.

Hofmann T, Obukhov AG, Schaefer M, Harteneck C, Gudermann T and Schultz G (1999) Direct activation of human TRPC6 and TRPC3 channels by diacylglycerol. *Nature* **397**:259–263.

Huang EJ and Reichardt LF (2001) Neurotrophins: roles in neuronal development and function. *Annu Rev Neurosci* **24**:677–736.

Huang EJ and Reichardt LF (2003) Trk receptors: roles in neuronal signal transduction. *Annu Rev Biochem* **72**:609–642.

Inoue R, Okada T, Onoue H, Hara Y, Shimizu S, Naitoh S, Ito Y and Mori Y (2001) The transient receptor potential protein homologue TRP6 is the essential component of vascular α_1-adrenoceptor-activated Ca^{2+}-permeable cation channel. *Circ Res* **88**:325–332.

Itsuki K, Imai Y, Hase H, Okamura Y, Inoue R and Mori MX (2014) PLC-mediated PI(4,5)P$_2$ hydrolysis regulates activation and inactivation of TRPC6/7 channels. *J Gen Physiol* **143**:183–201.

Jia Y, Zhou J, Tai Y and Wang Y (2007) TRPC channels promote cerebellar granule neuron survival. *Nat Neurosci* **10**:559–567.

Kamm KE and Stull JT (2001) Dedicated myosin light chain kinases with diverse cellular functions. *J Biol Chem* **276**:4527–4530.

Kiyonaka S, Kato K, Nishida M, Mio K, Numaga T, Sawaguchi Y, Yoshida T, Wakamori M, Mori E, Numata T, Ishii M, Takemoto H, Ojida A, Watanabe K, Uemura A, Kurose H, Morii T, Kobayashi T, Sato Y, Sato C, Hamachi I and Mori Y (2009) Selective and direct inhibition of TRPC3 channels underlies biological activities of a pyrazole compound. *Proc Natl Acad Sci U S A* **106**:5400–5405.

Leuner K, Heiser JH, Derksen S, Mladenov MI, Fehske CJ, Schubert R, Gollasch M, Schneider G, Harteneck C, Chatterjee SS and Muller WE (2010) Simple 2,4-diacylphloroglucinols as classic transient receptor potential-6 activators—identification of a novel pharmacophore. *Mol Pharmacol* **77**:368–377.

Leuner K, Kazanski V, Muller M, Essin K, Henke B, Gollasch M, Harteneck C and

Muller WE (2007) Hyperforin—a key constituent of St. John's wort specifically activates TRPC6 channels. *FASEB J* **21**:4101–4111.

Leuner K, Li W, Amaral MD, Rudolph S, Calfa G, Schuwald AM, Harteneck C, Inoue T and Pozzo-Miller L (2013) Hyperforin modulates dendritic spine morphology in hippocampal pyramidal neurons by activating Ca^{2+}-permeable TRPC6 channels. *Hippocampus* **23**:40–52.

Li HS, Xu XZ and Montell C (1999) Activation of a TRPC3-dependent cation current through the neurotrophin BDNF. *Neuron* **24**:261–273.

Li Y, Jia YC, Cui K, Li N, Zheng ZY, Wang YZ and Yuan XB (2005) Essential role of TRPC channels in the guidance of nerve growth cones by brain-derived neurotrophic factor. *Nature* **434**:894–898.

Meijering E, Jacob M, Sarria JC, Steiner P, Hirling H and Unser M (2004) Design and validation of a tool for neurite tracing and analysis in fluorescence microscopy images. *Cytometry A* **58**:167–176.

Merritt JE, Armstrong WP, Benham CD, Hallam TJ, Jacob R, Jaxa-Chamiec A, Leigh BK, McCarthy SA, Moores KE and Rink TJ (1990) SK&F 96365, a novel inhibitor of receptor-mediated calcium entry. *Biochem J* **271**:515–522.

Mori Y, Takahashi N, Polat OK, Kurokawa T, Takeda N and Inoue M (2015) Redox-sensitive transient receptor potential channels in oxygen sensing and adaptation. *Pflugers Arch* DOI: 10.1007/s00424-015-1716-2 [published ahead of print].

Nagahara AH and Tuszynski MH (2011) Potential therapeutic uses of BDNF in neurological and psychiatric disorders. *Nat Rev Drug Discov* **10**:209–219.

Nguyen T and Di Giovanni S (2008) NFAT signaling in neural development and axon

growth. *Int J Dev Neurosci* **26**:141–145.

Nilius B and Szallasi A (2014) Transient receptor potential channels as drug targets: from the science of basic research to the art of medicine. *Pharmacol Rev* **66**:676–814.

Nishizuka Y (1995) Protein kinase C and lipid signaling for sustained cellular responses. *FASEB J* **9**:484–496.

Numaga T, Nishida M, Kiyonaka S, Kato K, Katano M, Mori E, Kurosaki T, Inoue R, Hikida M, Putney JW, Jr. and Mori Y (2010) Ca^{2+} influx and protein scaffolding via TRPC3 sustain PKCβ and ERK activation in B cells. *J Cell Sci* **123**:927–938.

Okada T, Inoue R, Yamazaki K, Maeda A, Kurosaki T, Yamakuni T, Tanaka I, Shimizu S, Ikenaka K, Imoto K and Mori Y (1999) Molecular and functional characterization of a novel mouse transient receptor potential protein homologue TRP7: Ca^{2+}-permeable cation channel that is constitutively activated and enhanced by stimulation of G protein-coupled receptor. *J Biol Chem* **274**:27359–27370.

Onohara N, Nishida M, Inoue R, Kobayashi H, Sumimoto H, Sato Y, Mori Y, Nagao T and Kurose H (2006) TRPC3 and TRPC6 are essential for angiotensin II-induced cardiac hypertrophy. *EMBO J* **25**:5305–5316.

Park H and Poo MM (2013) Neurotrophin regulation of neural circuit development and function. *Nat Rev Neurosci* **14**:7–23.

Poduslo JF and Curran GL (1996) Permeability at the blood-brain and blood-nerve barriers of the neurotrophic factors: NGF, CNTF, NT-3, BDNF. *Brain Res Mol Brain Res* **36**:280–286.

Qu L, Li Y, Pan X, Zhang P, LaMotte RH and Ma C (2012) Transient receptor potential canonical 3 (TRPC3) is required for IgG immune complex-induced excitation of the rat dorsal root ganglion neurons. *J Neurosci* **32**:9554–9562.

Reading SA, Earley S, Waldron BJ, Welsh DG and Brayden JE (2005) TRPC3 mediates pyrimidine receptor-induced depolarization of cerebral arteries. *Am J Physiol Heart Circ Physiol* **288**:H2055–2061.

Reichardt LF (2006) Neurotrophin-regulated signalling pathways. *Philos Trans R Soc Lond B Biol Sci* **361**:1545–1564.

Ruchhoeft ML and Harris WA (1997) Myosin functions in Xenopus retinal ganglion cell growth cone motility in vivo. *J Neurobiol* **32**:567–578.

Russo E, Scicchitano F, Whalley BJ, Mazzitello C, Ciriaco M, Esposito S, Patane M, Upton R, Pugliese M, Chimirri S, Mammi M, Palleria C and De Sarro G (2014) Hypericum perforatum: pharmacokinetic, mechanism of action, tolerability, and clinical drug-drug interactions. *Phytother Res* **28**:643–655.

Saleh SN, Albert AP, Peppiatt CM and Large WA (2006) Angiotensin II activates two cation conductances with distinct TRPC1 and TRPC6 channel properties in rabbit mesenteric artery myocytes. *J Physiol* **577**:479–495.

Sell TS, Belkacemi T, Flockerzi V and Beck A (2014) Protonophore properties of hyperforin are essential for its pharmacological activity. *Sci Rep* **4**:7500.

Shaywitz AJ and Greenberg ME (1999) CREB: a stimulus-induced transcription factor activated by a diverse array of extracellular signals. *Annu Rev Biochem* **68**:821–861.

Shi J, Mori E, Mori Y, Mori M, Li J, Ito Y and Inoue R (2004) Multiple regulation by calcium of murine homologues of transient receptor potential proteins TRPC6

and TRPC7 expressed in HEK293 cells. *J Physiol* **561**:415-432.

Tai Y, Feng S, Ge R, Du W, Zhang X, He Z and Wang Y (2008) TRPC6 channels promote dendritic growth via the CaMKIV-CREB pathway. *J Cell Sci* **121**:2301–2307.

Takahashi N, Hamada-Nakahara S, Itoh Y, Takemura K, Shimada A, Ueda Y, Kitamata M, Matsuoka R, Hanawa-Suetsugu K, Senju Y, Mori MX, Kiyonaka S, Kohda D, Kitao A, Mori Y and Suetsugu S (2014) TRPV4 channel activity is modulated by direct interaction of the ankyrin domain to PI(4,5)P$_2$. *Nat Commun* **5**:4994.

Takahashi N, Mizuno Y, Kozai D, Yamamoto S, Kiyonaka S, Shibata T, Uchida K and Mori Y (2008) Molecular characterization of TRPA1 channel activation by cysteine-reactive inflammatory mediators. *Channels (Austin)* **2**:287–298.

Tao X, Finkbeiner S, Arnold DB, Shaywitz AJ and Greenberg ME (1998) Ca^{2+} influx regulates BDNF transcription by a CREB family transcription factor-dependent mechanism. *Neuron* **20**:709–726.

Uriu Y, Kiyonaka S, Miki T, Yagi M, Akiyama S, Mori E, Nakao A, Beedle AM, Campbell KP, Wakamori M and Mori Y (2010) Rab3-interacting molecule gamma isoforms lacking the Rab3-binding domain induce long lasting currents but block neurotransmitter vesicle anchoring in voltage-dependent P/Q-type Ca^{2+} channels. *J Biol Chem* **285**:21750–21767.

Vazquez G, Wedel BJ, Aziz O, Trebak M and Putney JW, Jr. (2004) The mammalian TRPC cation channels. *Biochim Biophys Acta* **1742**:21–36.

Venkatachalam K, Zheng F and Gill DL (2003) Regulation of canonical transient receptor potential (TRPC) channel function by diacylglycerol and protein kinase

C. *J Biol Chem* **278**:29031–29040.

Vohra PK, Thompson MA, Sathish V, Kiel A, Jerde C, Pabelick CM, Singh BB and Prakash YS (2013) TRPC3 regulates release of brain-derived neurotrophic factor from human airway smooth muscle. *Biochim Biophys Acta* **1833**:2953–2960.

Wayman GA, Lee YS, Tokumitsu H, Silva AJ and Soderling TR (2008) Calmodulin-kinases: modulators of neuronal development and plasticity. *Neuron* **59**:914–931.

Wolfle U, Seelinger G and Schempp CM (2014) Topical application of St. John's wort (Hypericum perforatum). *Planta Med* **80**:109–120.

Wu HY, Hudry E, Hashimoto T, Kuchibhotla K, Rozkalne A, Fan Z, Spires-Jones T, Xie H, Arbel-Ornath M, Grosskreutz CL, Bacskai BJ and Hyman BT (2010) Amyloid β induces the morphological neurodegenerative triad of spine loss, dendritic simplification, and neuritic dystrophies through calcineurin activation. *J Neurosci* **30**:2636–2649.

Yoshida T, Inoue R, Morii T, Takahashi N, Yamamoto S, Hara Y, Tominaga M, Shimizu S, Sato Y and Mori Y (2006) Nitric oxide activates TRP channels by cysteine S-nitrosylation. *Nat Chem Biol* **2**:596–607.

Zhang C, Roepke TA, Kelly MJ and Ronnekleiv OK (2008) Kisspeptin depolarizes gonadotropin-releasing hormone neurons through activation of TRPC-like cationic channels. *J Neurosci* **28**:4423–4434.

Zhang F, Kang Z, Li W, Xiao Z and Zhou X (2012) Roles of brain-derived neurotrophic factor/tropomyosin-related kinase B (BDNF/TrkB) signalling in Alzheimer's disease. *J Clin Neurosci* **19**:946–949.

Zheng JQ and Poo MM (2007) Calcium signaling in neuronal motility. *Annu Rev Cell*

Dev Biol **23**:375–404.

Footnotes

To whom reprint requests may be addressed at Yasuo Mori; Laboratory of Molecular Biology, Department of Synthetic Chemistry and Biological Chemistry, Graduate School of Engineering, Kyoto University, Katsura Campus, Nishikyo-ku, Kyoto 615-8510, Japan; E-mail, mori@sbchem.kyoto-u.ac.jp

Figure Legends

Fig. 1. Chemical structures of DAG-activated TRPC channels activators (A) Chemical structures of DAG, the DAG analogue OAG, hyperforin, and the hyperforin analogue Hyp9. (B) Chemical structures of piperazine-derived activators (compound 1–9) of DAG-activated TRPC channels.

Fig. 2. Screening of small molecule activators of the TRPC6 channel. (A) The principle of the FMP assay to detect TRPC6 channel activation. TRPC6 channel activators induce influx of cations such as Na^+ and Ca^{2+} from the extracellular solution, leading to membrane potential depolarization. In response to the depolarization, the FMP probe translocates to the cytoplasm from the extracellular space and exhibits increased its fluorescence intensity. (B) Time courses of FMP probe fluorescence after addition of CCh to HEK 293 cells stably expressing TRPC6 (a.u., arbitrary units). (C and D) Representative traces of fluorescence changes induced by the compound 1 (PPZ1) (C) or compound 6 (PPZ2) (D) in vector-transfected cells and TRPC3- or TRPC6-expressing cells. The compounds were added at 1 second after beginning the observation. (E) Maximum increases in $[Ca^{2+}]_i$ ($\Delta[Ca^{2+}]_i$) induced by addition of the nine identified activators, each at 10 μM, for 8 minutes in HEK 293 cells transfected with TRPC3, TRPC6, TRPC7, or vector (n = 24–80). $^*P < 0.05$; $^{**}P < 0.01$; $^{***}P < 0.001$ compared with vector. Data points show the means ± S.E.M.

Fig. 3. Characterization of TRPC channel activation by PPZ1 and PPZ2 based on $[Ca^{2+}]_i$ measurements. (A and B) $[Ca^{2+}]_i$ changes induced by PPZ1 (A) and PPZ2 (B) in HEK 293 cells expressing TRPC subtypes TRPC1–C7, respectively. Averaged time

52

courses and $\Delta[Ca^{2+}]_i$ ($n = 25$–99). [***]$P < 0.001$, as compared with vector. (C and D) Dose-response relationships for $\Delta[Ca^{2+}]_i$ induced by PPZ1 (C) and PPZ2 (D) in HEK 293 cells expressing TRPC3, TRPC5, TRPC6, TRPC7 or vector ($n = 17$–169). (E–H) Effects of 5 μM U73122 or U73343 on $[Ca^{2+}]_i$ increases induced by 100 μM PPZ1 (E and F) and 30 μM PPZ2 (G and H) in HEK 293 cells expressing TRPC3, TRPC6 and TRPC7. Averaged time courses of $[Ca^{2+}]_i$ changes in TRPC7-expressing cells and $\Delta[Ca^{2+}]_i$ in TRPC3-, TRPC6- and TRPC7-expressing cells ($n = 21$–48) are shown. n.s., not significant compared to DMSO or U73343. Data points show the means ± S.E.M.

Fig. 4. Electrophysiological characterization of TRPC3, TRPC6, and TRPC7 channel activation by PPZ1 and PPZ2. (A and B) Whole-cell patch clamp recordings of ionic currents evoked by 100 μM PPZ1 (A) and 30 μM PPZ2 (B) in HEK 293 cells transfected with TRPC3, TRPC6, TRPC7, or vector. Representative traces of inward and outward currents recorded at –100 and +100 mV, respectively, under ramp clamp (top rows). Corresponding *I-V* relationships at the time points 1 and 2 (bottom rows). (C and D) Peak current densities at –100 and +100 mV during the application of 100 μM PPZ1 (C) and 30 μM PPZ2 (D) ($n = 8$–19). [*]$P < 0.05$; [**]$P < 0.01$; [***]$P < 0.001$ compared with vector. Data points show the means ± S.E.M.

Fig. 5. Whole-cell currents evoked by PPZ2 in rabbit portal vein smooth muscle cells. (A) Representative traces of the currents activated by 10 μM Norad and PPZ2 recorded at –66 mV. (B) Corresponding *I-V* relationships at the time points of 1, 2, and 3. (C) Peak current densities induced by PPZ2 normalized to that of 10 μM Norad ($n = 4$–13). Data points show the means ± S.E.M.

Fig. 6. Neurite outgrowth promotion by PPZ1 and PPZ2 in cultured neurons. (A) RT-PCR analysis for mRNA expression of TRPC channels in CGNs at 1 day *in vitro* (at 1 DIV). (B) Representative fluorescence images of CGNs stained with the neuronal marker MAP2 (green) and the morphological indicator F-actin (red). CGNs were treated with 0.1% DMSO, 50 ng/ml BDNF, 10 nM PPZ1 or 10 nM PPZ2 for 24 hours and fixed at 1 DIV. (C) Total neurite length relative to that in DMSO-treated control cells in response to 50 ng/ml BDNF or PPZ1 and PPZ2 at various concentrations, as indicated (n = 32–127). $^{*}P < 0.05$; $^{**}P < 0.01$; $^{***}P < 0.001$ compared with DMSO. (D) Effects of TRPC inhibition by 0.3 μM Pyr3 and 1 μM Pyr4 on PPZ1- or PPZ2-induced promotion of neurite outgrowth in CGNs (n = 44–92). $^{*}P < 0.05$; $^{**}P < 0.01$; $^{***}P < 0.001$ compared with DMSO. (E) RT-PCR analyses of TRPC3, TRPC6 and TRPC7 expression in CGNs electroporated with a randomized siRNA (siControl) or an siRNA mixture targeting TRPC3, TRPC6, and TRPC7 (siTRPC3/6/7). (F) Effects of TRPC knockdown on 10 nM PPZ1- or PPZ2-induced promotion of neurite outgrowth in CGNs (n = 66–120). $^{*}P < 0.05$; $^{**}P < 0.01$; $^{***}P < 0.001$, compared with siControl or DMSO. (G) Total neurite length of cultured hippocampal neurons, relative to DMSO-treated control neurons, in response to 50 ng/ml BDNF or PPZ1 and PPZ2 at the indicated concentrations (n = 22–32). $^{*}P < 0.05$; $^{***}P < 0.001$, compared with DMSO. (H) The effects of 1 μM SK&F 96365 (SKF), 1 μM Pyr4, and 0.1 μM capsazepine (CPZ) on 50 ng/ml BDNF-, 100 nM PPZ1- or 100 nM PPZ2-induced neurite outgrowth in hippocampal neurons (n = 38–98). $^{*}P < 0.05$; $^{**}P < 0.01$; $^{***}P < 0.001$, compared with DMSO. Data points show the means ± S.E.M.

54

Fig. 7. (A) A representative trace of whole-cell currents induced by 30 μM PPZ2 in CGNs recorded at –60 mV. (B) Corresponding *I-V* relationships at the time points of 1 and 2. (C) The *I-V* relationship for the PPZ2-induced currents was obtained by subtraction in (B). (D) Averaged peak current densities of CGNs before (control) and after application of PPZ2 at –60 mV (*n* = 11–14). $^{*}P < 0.05$, compared with control. (E) Representative traces of whole-cell currents induced by 10 and 30 μM PPZ2 in CGNs transfected with siControl or siTRPC3/6/7 at –60 mV. (F) Averaged peak current densities of CGNs transfected with siControl or siTRPC3/6/7 before and after application of PPZ2 at –60 mV (n = 5–8). $^{*}P < 0.05$. Data points show the means ± S.E.M.

Fig. 8. Neurite growth-promoting effects of PPZ1 and PPZ2 via Ca^{2+}-dependent signaling in CGNs. (A–C) 30 μM PPZ2-induced Ca^{2+} responses in cultured CGNs at 1 DIV. Representative averaged time courses in 2 mM Ca^{2+}-containing (A) or Ca^{2+}-free, 0.5 mM EGTA-containing (B) external solutions and averaged $\Delta[Ca^{2+}]_i$ (C) (*n* = 92–248). $^{*}P < 0.05$; $^{**}P < 0.01$; $^{***}P < 0.001$, compared with DMSO. (D) Total neurite outgrowth of CGNs treated for 24 hours with 0.1% DMSO, 50 ng/ml BDNF, 10 nM PPZ1 or with 10 nM PPZ2 alone or in combination with various inhibitors of Ca^{2+}-dependent signaling, as indicated. Mean values of total neurite length were normalized to those in DMSO-treated control cells without inhibitors. CGNs were fixed at 1 DIV (*n* = 22–137). $^{*}P < 0.05$; $^{**}P < 0.01$; $^{***}P < 0.001$, compared with DMSO. (E) PPZ2-induced CREB phosphorylation detected by western blotting (WB) using a Ser-133-phosphorylated CREB-specific antibody and a total CREB antibody. Cultured CGNs at 1 DIV were treated with DMSO or 10 μM PPZ2 for the indicated

times and lysed. Total cell lysates were subjected to western blotting. (F) CREB phosphorylation was quantified as the ratio of the amount of phosphorylated CREB to the total amount of CREB. Mean ratios were normalized to the ratio of the cells treated with 0.1% DMSO for 15 min ($n = 3$–4). $^{**}P < 0.01$, compared with DMSO. Data points show the means ± S.E.M.
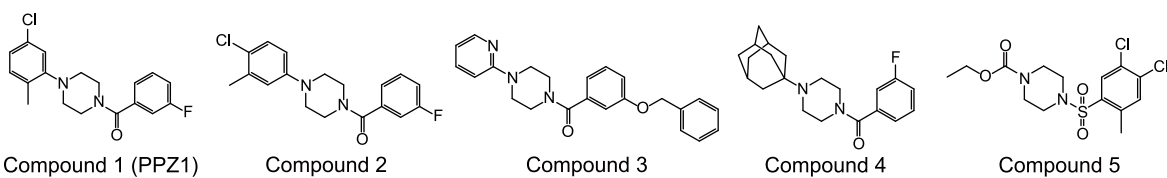
Fig. 9. Neuroprotective effects of PPZ1 and PPZ2 on cultured CGNs. (A) Representative images of CGNs treated with 0.1% DMSO, 50 ng/ml BDNF, 100 nM PPZ1 or 10 nM PPZ2 were obtained by staining with the nuclear marker Hoechst33342 (Hoechst) (blue) and dead cell marker PI (red). Scale bar, 100 μm. (B) Percentages of PI-positive CGNs treated with DMSO, BDNF, PPZ1 or PPZ2 ($n = 20$–47). $^{*}P < 0.05$; $^{**}P < 0.01$; $^{***}P < 0.001$, compared with DMSO. Cell death was induced in CGNs by 24 hours serum deprivation. Cells were pretreated with 0.1% DMSO, 50 ng/ml BDNF, PPZ1 or PPZ2 for 24 hours prior to serum deprivation. (C) Effects of TRPC inhibition by 1 μM Pyr4 on neuroprotection induced by 50 ng/ml BDNF, 100 nM PPZ1 and 10 nM PPZ2 ($n = 18$–40). $^{*}P < 0.05$; $^{**}P < 0.01$; $^{***}P < 0.001$ compared with DMSO. Data points show the means ± S.E.M.

A

DAG

OAG

Hyperforin

Hyp9
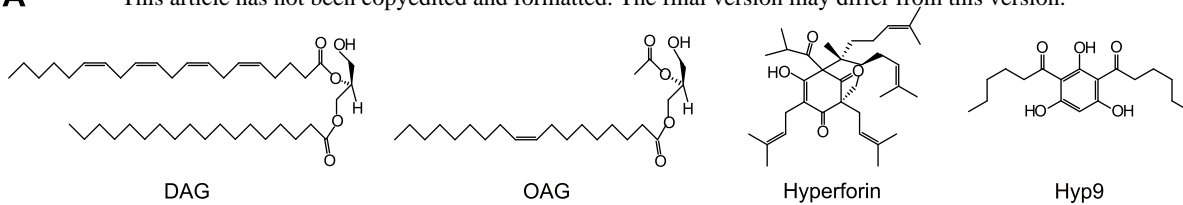
B

Group A : Benzoyl-piperazine and Sulfonyl piperazine derivatives

Compound 1 (PPZ1)

Compound 2

Compound 3

Compound 4

Compound 5

Group B : 1-Phenyl-piperazine-4-acetamide derivatives
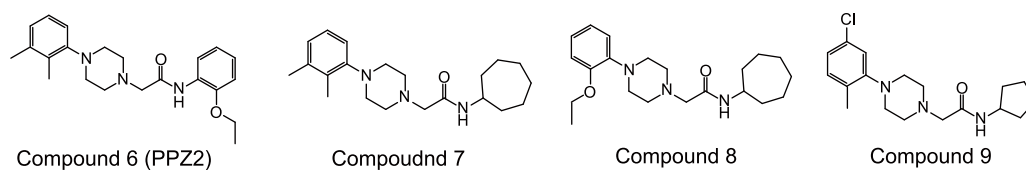
Compound 6 (PPZ2)

Compoudnd 7

Compound 8

Compound 9
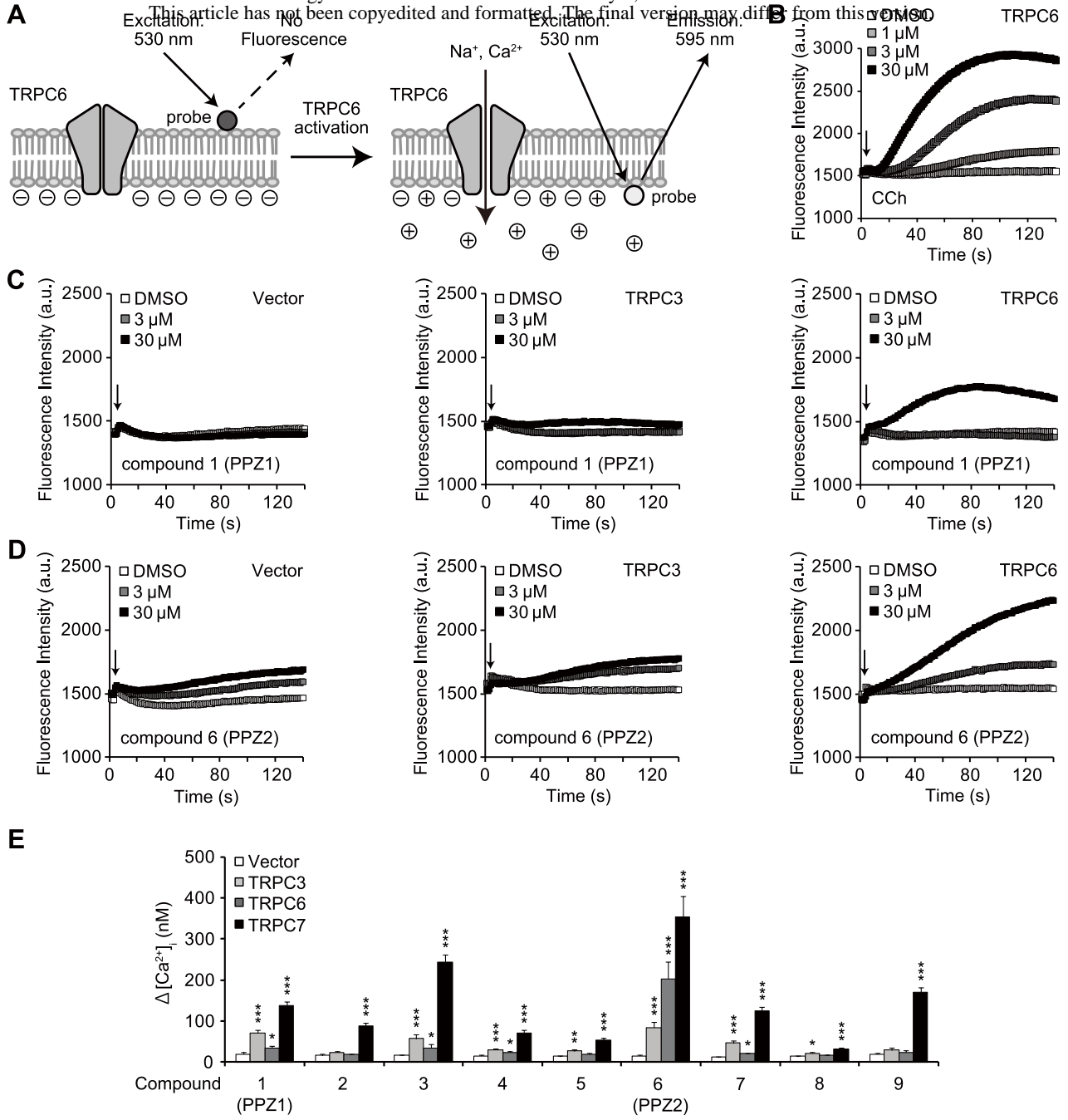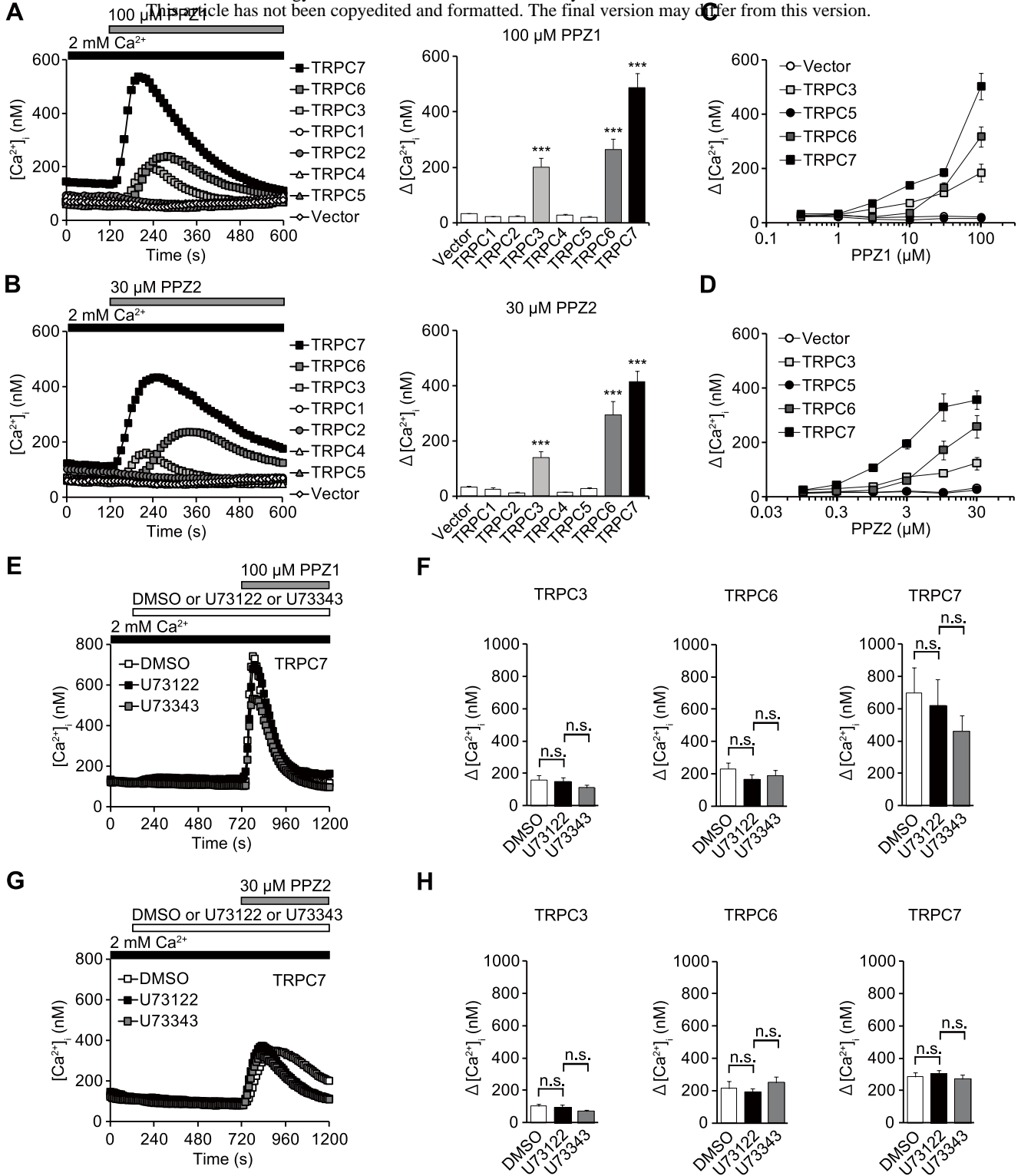
Figure 1
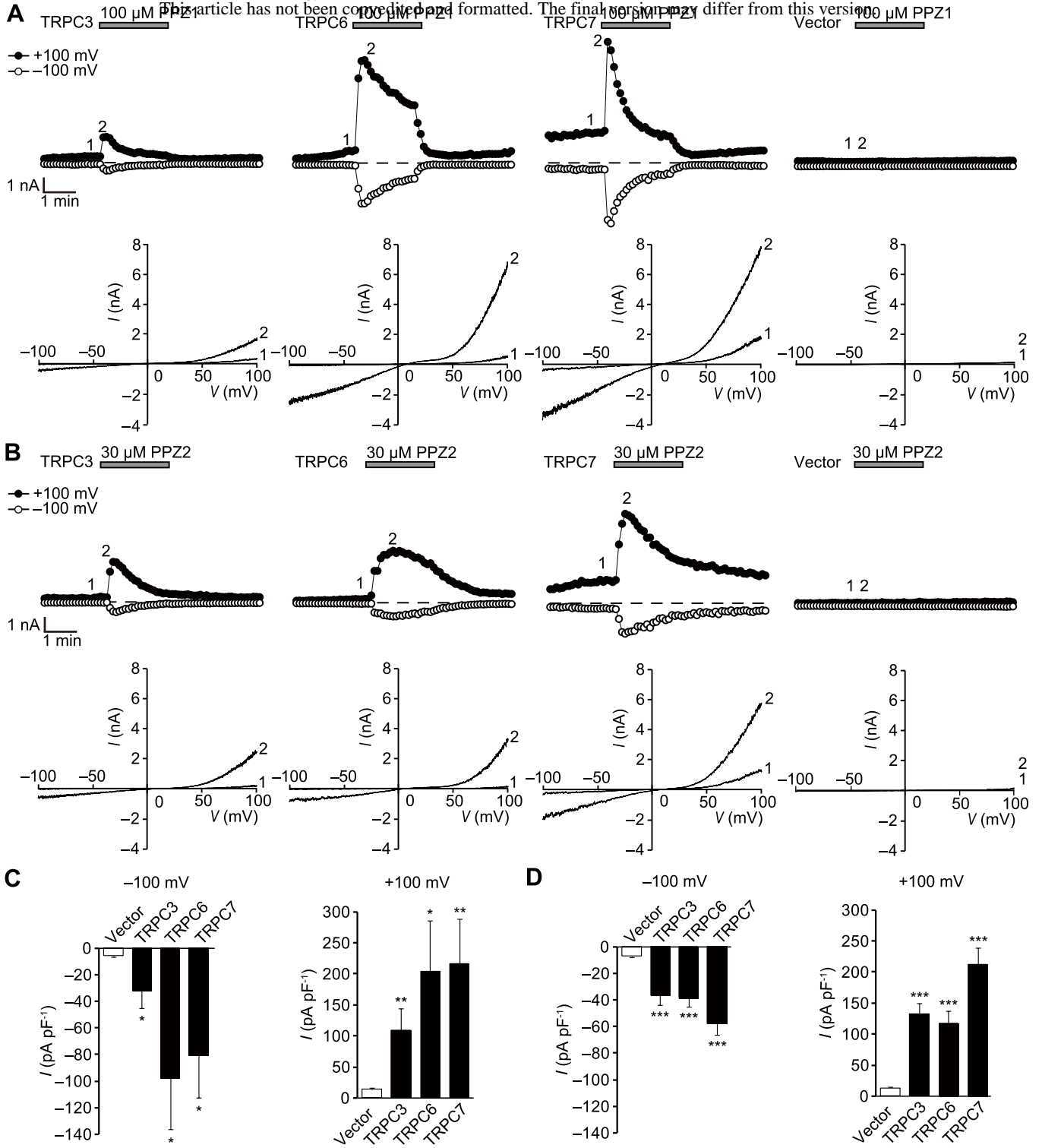
Figure 2

Figure 3

Figure 4
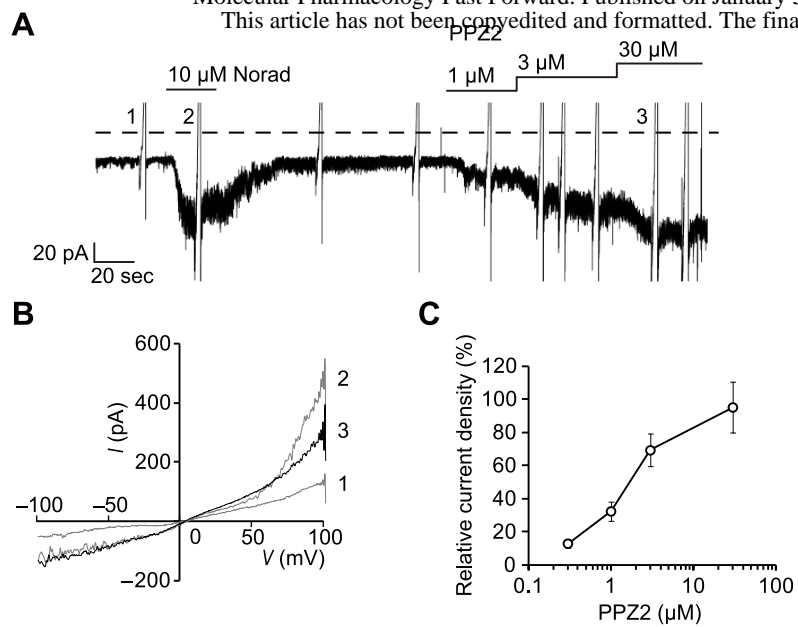
Figure 5
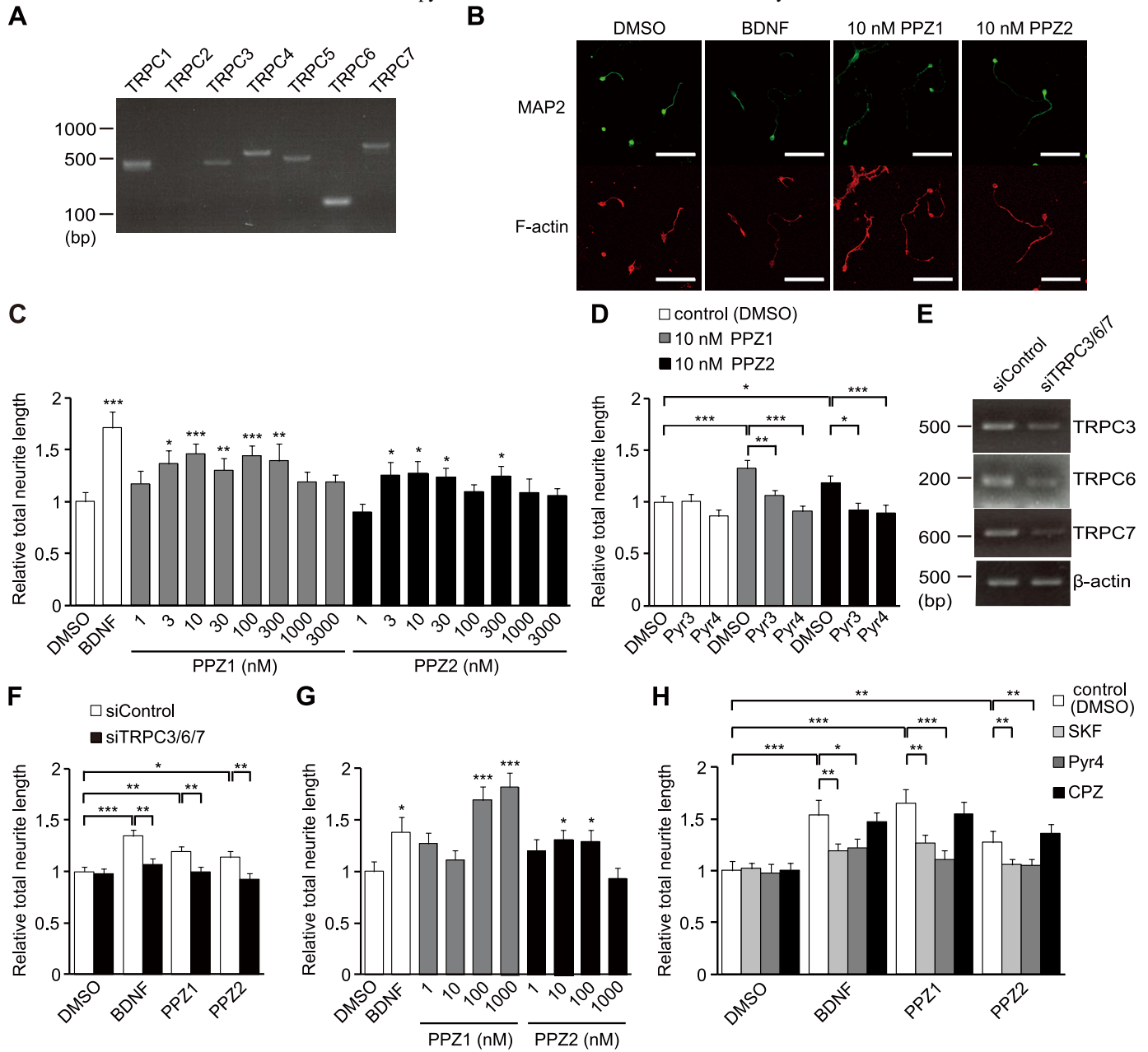
Figure 6
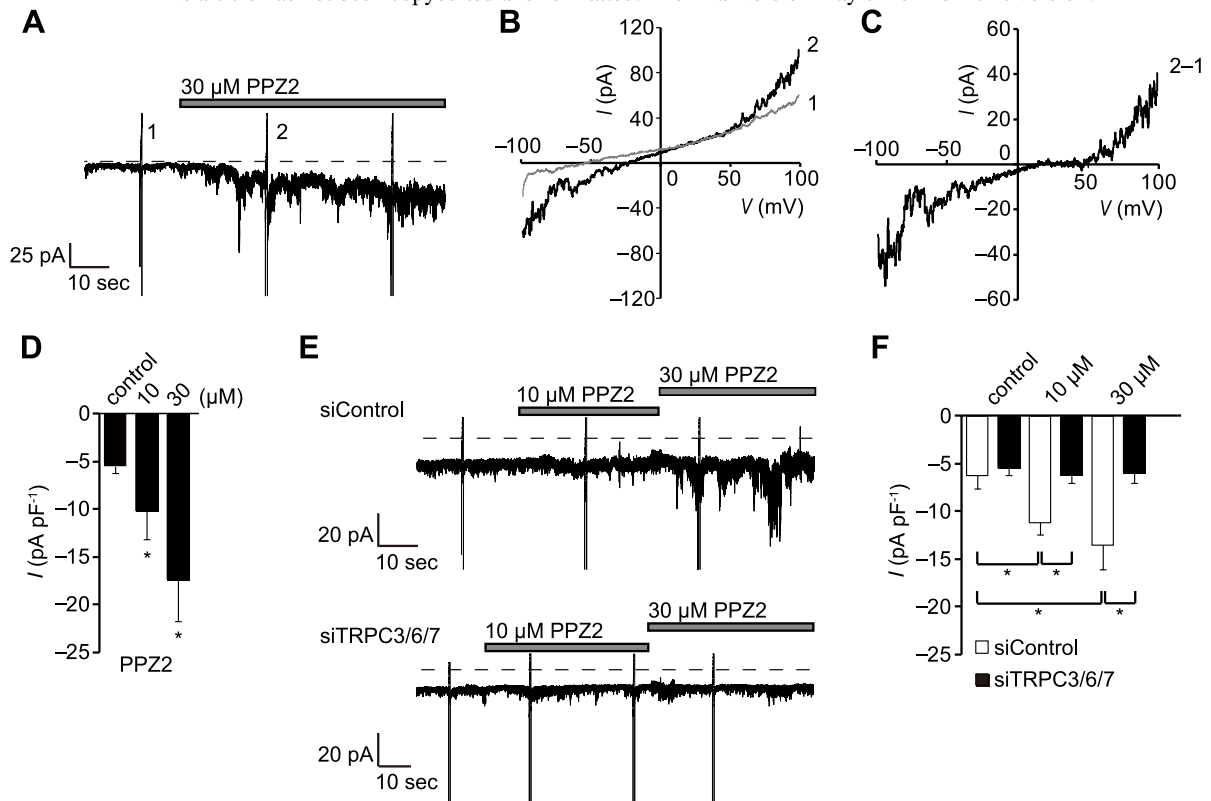
Figure 7

Figure 8

Figure 9